Article

Cell Reports

# Imbalance of Excitatory/Inhibitory Neuron Differentiation in Neurodevelopmental Disorders with an *NR2F1* Point Mutation

## Graphical Abstract

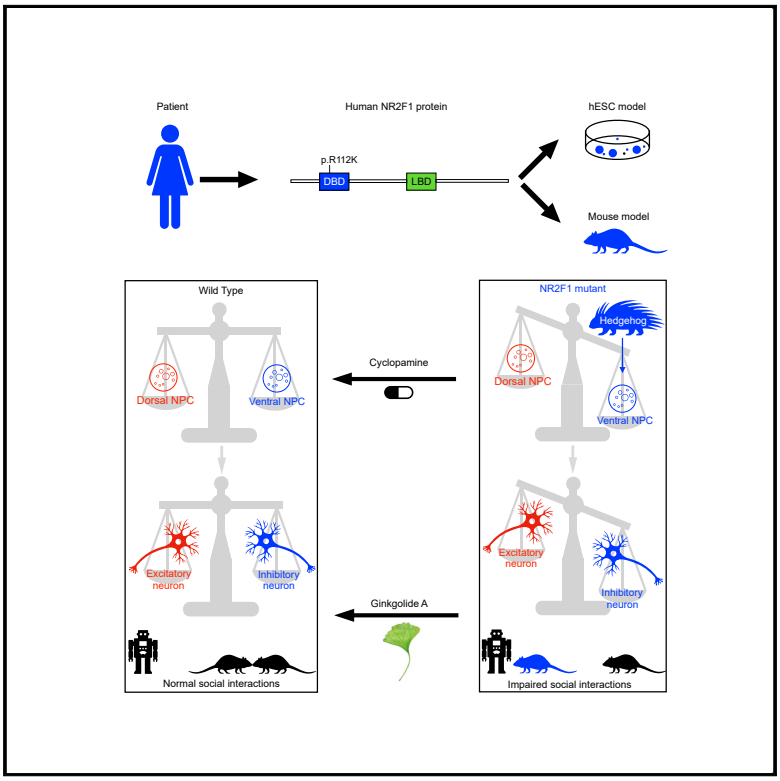


## Authors

Ke Zhang, Fang Yu, Jian Zhu, ..., Shuijin He, Naihe Jing, Ke Tang

## Correspondence

heshj@shanghaitech.edu.cn (S.H.), njing@sibcb.ac.cn (N.J.), tangke@gzhu.edu.cn (K.T.)

## In Brief

Zhang et al. find that a NR2F1-R112K mutation promotes inhibitory neuron differentiation by activating the Hedgehog signaling pathway, and corresponding mutant mice display behavioral deficits related to neurodevelopmental disorders, including autistic spectrum disorder (ASD), which could be partially alleviated by antagonizing the inhibitory synaptic transmission.

## Highlights

- NR2F1-R112K mutation causes excitatory and inhibitory neuron imbalance
- Activation of the Hedgehog pathway mainly accounts for the imbalance
- $Nr2f1^{+/m}$ mice display behavioral deficits of neurodevelopmental disorder, such as ASD
- Ginkgolide A treatment partially alleviates behavioral deficits of $Nr2f1^{+/m}$ mice

Zhang et al., 2020, Cell Reports *31*, 1–18
April 21, 2020 
https://doi.org/10.1016/j.celrep.2020.03.085

CellPress

Cell Reports
Article



# Imbalance of Excitatory/Inhibitory Neuron Differentiation in Neurodevelopmental Disorders with an *NR2F1* Point Mutation

Ke Zhang,[1,10] Fang Yu,[1,10] Jian Zhu,[2,10] Sue Han,[3,10] Jiehui Chen,[1,10] Xuanyuan Wu,[4,10] Yingying Chen,[1] Tingyu Shen,[3] Jiaoyang Liao,[1] Wenke Guo,[1] Xianfa Yang,[1,7] Ran Wang,[1] Yun Qian,[1] Jiaxin Yang,[2] Leping Cheng,[3,5] Yun Zhao,[1] Chi-Chung Hui,[6] Jinsong Li,[1] Guangdun Peng,[7,8,9] Shuijin He,[4,*] Naihe Jing,[1,4,7,8,9,11,*] and Ke Tang[2,*]

[1]State Key Laboratory of Cell Biology, CAS Center for Excellence in Molecular Cell Science, Shanghai Institute of Biochemistry and Cell Biology, Chinese Academy of Sciences, University of Chinese Academy of Sciences, Shanghai 200031, China
[2]Precise Genome Engineering Center, School of Life Sciences, Guangzhou University, Guangzhou, Guangdong 510006, China
[3]State Key Laboratory of Neuroscience, CAS Center for Excellence in Brain Science and Intelligence Technology, Institute of Neuroscience, Chinese Academy of Sciences, University of Chinese Academy of Sciences, Shanghai 200031, China
[4]School of Life Science and Technology, ShanghaiTech University, Shanghai 201210, China
[5]Key Laboratory of Longevity and Aging-related Diseases of Chinese Ministry of Education, Guangxi Collaborative Innovation Center for Biomedicine and Guangxi Key Laboratory of Regenerative Medicine, School of Preclinical Medicine, Guangxi Medical University, Nanning, Guangxi 530021, China
[6]Program in Developmental & Stem Cell Biology, Research Institute, Hospital for Sick Children, Toronto, ON M5G 0A4, Canada
[7]CAS Key Laboratory of Regenerative Biology, Guangdong Provincial Key Laboratory of Stem Cell and Regenerative Medicine, Guangzhou Institutes of Biomedicine and Health, Chinese Academy of Sciences, Guangzhou, Guangdong 510530, China
[8]Center for Cell Lineage and Atlas, Guangzhou Regenerative Medicine and Health Guangdong Laboratory (GRMH-GDL), Guangzhou, Guangdong 510005, China
[9]Institute for Stem Cell and Regeneration, Chinese Academy of Sciences, Beijing 100101, China
[10]Senior author
[11]Lead Contact
*Correspondence: heshj@shanghaitech.edu.cn (S.H.), njing@sibcb.ac.cn (N.J.), tangke@gzhu.edu.cn (K.T.)
https://doi.org/10.1016/j.celrep.2020.03.085

## SUMMARY

**Recent studies have revealed an essential role for embryonic cortical development in the pathophysiology of neurodevelopmental disorders, including autism spectrum disorder (ASD). However, the genetic basis and underlying mechanisms remain unclear. Here, we generate mutant human embryonic stem cell lines (Mut hESCs) carrying an NR2F1-R112K mutation that has been identified in a patient with ASD features and investigate their neurodevelopmental alterations. Mut hESCs overproduce ventral telencephalic neuron progenitors (ventral NPCs) and underproduce dorsal NPCs, causing the imbalance of excitatory/inhibitory neurons. These alterations can be mainly attributed to the aberrantly activated Hedgehog signaling pathway. Moreover, the corresponding *Nr2f1* point-mutant mice display a similar excitatory/inhibitory neuron imbalance and abnormal behaviors. Antagonizing the increased inhibitory synaptic transmission partially alleviates their behavioral deficits. Together, our results suggest that the NR2F1-dependent imbalance of excitatory/inhibitory neuron differentiation caused by the activated Hedgehog pathway is one precursor of neurodevelopmental disorders and may enlighten the therapeutic approaches.**

## INTRODUCTION

Genetic mutations contribute significant risk to neurodevelopmental disorders, such as autism spectrum disorder (ASD). More than 1,000 ASD candidate genes have been identified according to the Simons Foundation Autism Research Initiative (SFARI) database (Abrahams et al., 2013). Previous studies have illustrated that many genetic mutations disrupt excitatory/inhibitory synaptic assembly or transmission, which leads to an imbalance between excitatory and inhibitory neurons (E/I imbalance) (Casanova et al., 2003; Rubenstein, 2010; Südhof, 2008; Zoghbi and Bear, 2012). However, these mutations are heterogeneous, each accounting for fewer than 2% of cases, and about 80% of ASD patients have no clear etiology (Betancur, 2011; Geschwind, 2009). Exploration of additional genetic mutations, as well as the underlying mechanisms, could contribute to improved understanding of neurodevelopmental disorders, including ASD.

Recent data suggest that the common pathophysiology of a large proportion of ASD patients originates from abnormal embryonic cortical development (Adhya et al., 2019; Mariani et al., 2015; Parikshak et al., 2013; Willsey et al., 2013); however, the underlying mechanisms are still unclear. The specification of dorsal or ventral telencephalon, which determines excitatory or inhibitory neuron differentiation, is an essential biological event in embryonic cortical development (Marín and Rubenstein, 2001; Molyneaux et al., 2007; Wonders and Anderson, 2006). It raises a hypothesis that the dysregulated specification of

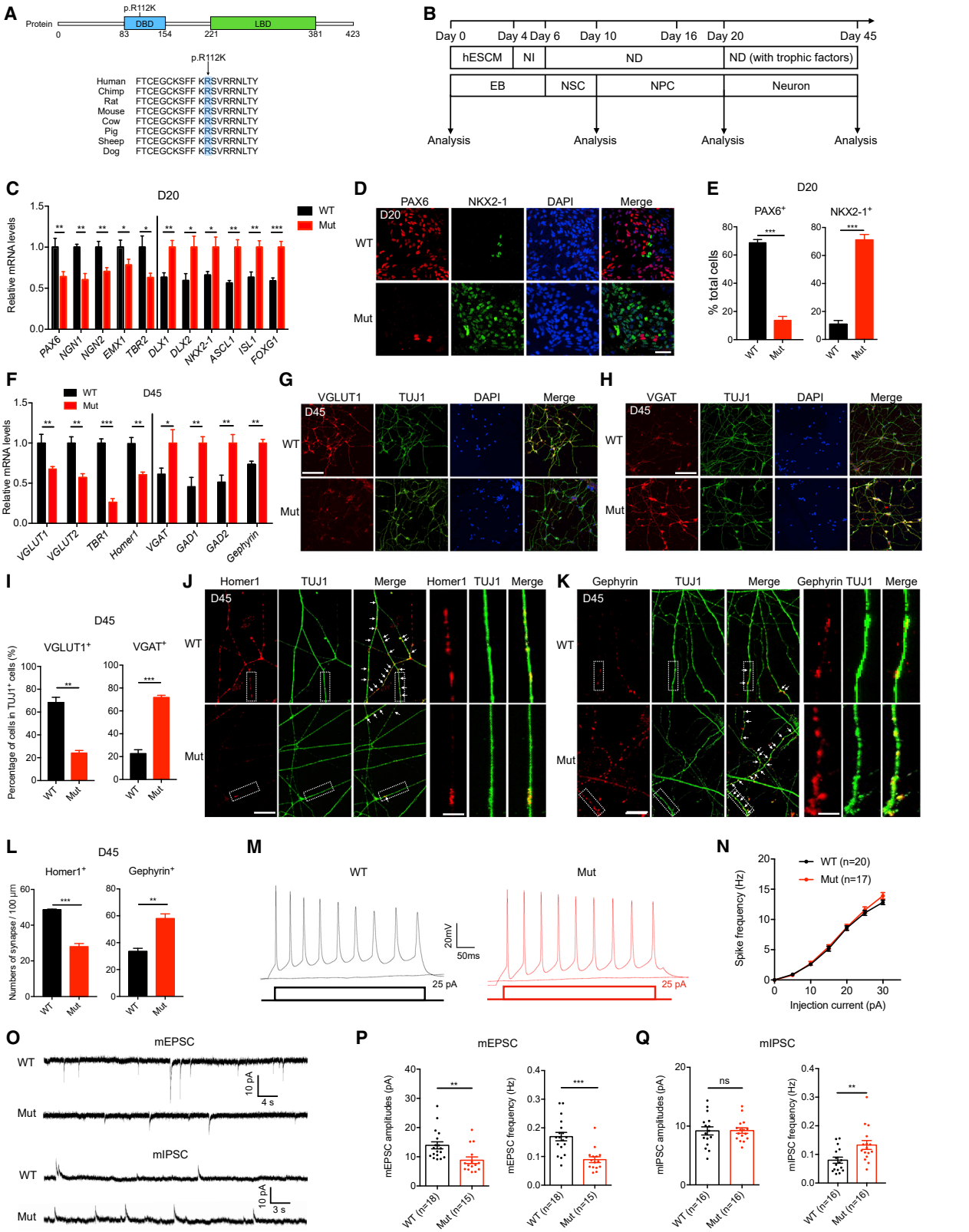


*(legend on next page)*

dorsal-ventral telencephalic neuron progenitor cells (NPCs) leads to an imbalance of excitatory/inhibitory neuron differentiation, which may underlie the E/I imbalance in neurodevelopmental disorders, especially ASD.

Nr2f1 is a critical transcription factor that determines mouse telencephalic development (Naka et al., 2008). It regulates not only cortical regionalization and excitatory projection neuron differentiation in dorsal telencephalon (Alfano et al., 2011; Armentano et al., 2007; O'Leary and Nakagawa, 2002; Zhou et al., 1999, 2001) but also inhibitory interneuron development in ventral telencephalon (Hu et al., 2017; Kessaris et al., 2014). However, little is known about the role of the *NR2F1* gene in human brain development and neurodevelopmental disorders. Human *NR2F1* mutations were initially identified in Bosch-Boonstra-Schaaf optic atrophy syndrome (BBSOAS), a neurodevelopmental disorder (Bosch et al., 2014; Chen et al., 2016). Moreover, recent genomic data have unveiled many *NR2F1* mutations in ASD patients (Chen et al., 2017; De Rubeis et al., 2014; Lim et al., 2017; Sanders et al., 2012). These results imply that *NR2F1* variants confer high susceptibility to neurodevelopmental disorders. Notably, one patient with a point mutation in the *NR2F1* gene (GRCh38.p12; chr5:93585358G>A; c.335G>A; p.R112K) was the first reported to manifest ASD features (Bosch et al., 2014). As no other deleterious mutations have been identified in this patient, the potential role and underlying mechanism of the NR2F1-R112K mutation in the pathogenesis of neurodevelopmental disorders awaits further investigation.

Here, we derive mutant human embryonic stem cells lines (Mut hESCs) containing the NR2F1-R112K mutation. Mut hESCs display overproduction of ventral NPCs and underproduction of dorsal NPCs, leading to an E/I imbalance. The above phenotypes are mainly attributed to Hedgehog pathway activation. Corresponding heterozygous *Nr2f1*-point mutant mice exhibit a similar E/I imbalance in the primary somatosensory cortex and display impaired social interactions, repetitive behaviors, learning and memory deficits, and anxiety. Moreover, we demonstrate that antagonizing the increased inhibitory synaptic transmission partially alleviates behavioral deficits in these mice.

## RESULTS

### Generation of Mut hESCs with the NR2F1-R112K Mutation

Mut hESCs harboring the point mutation (NR2F1-R112K) were generated by using the CRISPR-Cas9 system (Ran et al., 2013) (Figures 1A and S1A). Repeated efforts failed to generate heterozygous mutant lines, so homozygous mutant hESC lines were used to examine the effects of the NR2F1-R112K mutation. In total, three homozygous mutant lines and three isogenic wild-type H9 hESC lines (WT hESCs) were obtained. To examine off-target effects, we analyzed top potential off-target sites and found them intact (Table S1), suggesting faithful gene editing by the CRISPR-Cas9 system in hESCs, as reported earlier (Smith et al., 2014; Veres et al., 2014). We then subjected both wild-type (WT) and Mut hESCs into cortical neuron differentiation to mimic embryonic telencephalic development by using a modified serum-free embryonic body (SFEB) method (Figure 1B) (Elkabetz et al., 2008; Li et al., 2017a; Zhang et al., 2001). The neuron differentiation process was divided into consecutive stages: pluripotency (day 0 [D0]), differentiation initiation (D2–D6), neural commitment (D8–D10), neuron progenitor cell proliferation (D12–D20), and neuron differentiation-maturation stage (D22–D45). The neuron differentiation process was analyzed at four representative time points (D0, D10, D20, and D45) (Figure 1B).

### Mut hESCs Preferentially Differentiate into Ventral Telencephalic NPCs and Inhibitory Neurons

At D0, the levels of transcripts and proteins of pluripotent markers (*OCT4*, *NANOG*, *REX1*, and *SOX2*) (Rogers et al., 1991; Shi et al., 2006; Takahashi et al., 2007) displayed high similarity between WT and Mut cells (Figures S1B–S1D). We also observed no significant changes in the expression of neural stem cell (NSC) markers (*PAX6*, *SOX2*, *OTX2*, *POU3F1/OCT6*,

**Figure 1. Mut hESCs Preferentially Differentiate into Ventral Telencephalic NPCs and Inhibitory Neurons**

(A) Top: an illustration of the human NR2F1 protein structure. The wild-type (WT) human NR2F1 protein has 423 amino acids, the point mutation (GRCh38.p12; chr5:93585358G>A; c.335G>A; p.R112K) locates in the DNA-binding domain. P, protein; R, arginine; K, lysine; DBD, DNA-binding domain; LBD, ligand-binding domain. Bottom: the sequence alignment showing the evolutionary conservation of the amino acid residues.

(B) The schematic procedure of cortical neuron differentiation of hESCs. hESCM, human embryonic stem cells growth medium; NI, neural induction medium; ND, neuron differentiation medium; EB, embryonic body; NSC, neural stem cell; NPC, neuron progenitor cell. The details are described in STAR Methods.

(C) The relative RNA expression levels of dorsal (*PAX6*, *NGN1*, *NGN2*, *EMX1*, and *TBR2*) and ventral (*DLX1*, *DLX2*, *NKX2-1*, *ASCL1*, *ISL1*, and *FOXG1*) NPC markers at D20. Expression is normalized to glyceraldehyde-3-phosphate dehydrogenase (GAPDH) and WT or Mut levels.

(D and E) Immunostaining (D) and quantification (E) of dorsal (PAX6) and ventral (NKX2-1) NPC markers at D20.

(F) The relative RNA expression levels of excitatory (*VGLUT1*, *VGLUT2*, *TBR1*, and *Homer1*) and inhibitory (*VGAT*, *GAD1*, *GAD2*, and *Gephyrin*) neuron or synapse markers at D45. The expression is normalized to GAPDH and WT or Mut levels.

(G–I) Immunostaining (G) and quantification (I) of excitatory (VGLUT1) or inhibitory (VGAT) (H and I) neuron or synapse markers at D45. TUJ1, a pan-neuronal marker.

(J–L) Immunostaining (J) and quantification (L) of excitatory (Homer1) or inhibitory (Gephyrin) (K and L) neuron or synapse markers at D45. Scale bar, 5 μm. Close-ups of the outlined region displaying Homer1 or Gephyrin puncta. Scale bar, 1 μm.

(M) Representative recording traces depicting the membrane voltage deflection of neurons at D65 in response to the step current injections of 0 pA and 25 pA with a 500-ms duration.

(N) The plot of evoked action potential rates versus the magnitude of injected current (input-output curve) from neurons at D65.

(O–Q) Representative recordings (O) and quantification (P) of mEPSCs and mIPSCs (O and Q) from neurons at D65.

Data are presented as means ± SEM; n represents the numbers of neuron differentiation with three lines, one experiment of neuron differentiation per line in (C), (E), (F), (I), and (L); n represents the numbers of recorded neurons in (N), (P), and (Q); Student's t test analysis is used in (C), (E), (F), (I), (L), (N), (P), and (Q). Scale bar, 30 μm (D) and 50 μm (G and H).

See also Figures S1 and S2 and Table S1.

and *ZNF521*) (Ellis et al., 2004; Qiao et al., 2015; Zhang et al., 2010; Zhu et al., 2014) at D10 (Figures S1E–S1G). Moreover, the expression levels of pan-NPC markers (*MUSASHI-1*, *FABP7*, *SOX1*, *GFAP*, and *VIMENTIN*) (Farkas et al., 2003; Garcia et al., 2004; Kaneko et al., 2000; Pankratz et al., 2007) were comparable between WT and Mut cells at D20 (Figures S1H–S1J). These results suggest that both WT and Mut hESCs have an equivalent potential to differentiate into NPCs.

It has been demonstrated that the specification of dorsal-ventral telencephalic NPCs is essential to brain development (Campbell, 2003; Wilson and Rubenstein, 2000) and that the mouse *Nr2f1* gene is involved in both dorsal and ventral telencephalic development (Alfano et al., 2011; Armentano et al., 2007; Hu et al., 2017; Naka et al., 2008; Zhou et al., 1999; Zhou et al., 2001). To investigate whether the NR2F1-R112K mutation affects the dorsal-ventral specification in human NPCs, we examined the expression of dorsal and ventral NPC markers at D20. Consistent with previous studies (Li et al., 2009; Li et al., 2017a), dorsal NPC markers (*PAX6*, *NGN1*, *NGN2*, *EMX1*, and *TBR2*) (Bulfone et al., 1999; Fode et al., 2000; Hevner et al., 2006) were highly expressed in WT NPCs at D20 (Figure 1C), implying their dorsal telencephalic NPC identities. Strikingly, Mut NPCs displayed much higher levels of RNA expression of ventral NPC markers (*DLX1*, *DLX2*, *NKX2-1*, *ASCL1*, *ISL1*, and *FOXG1*) (Fode et al., 2000; Mariani et al., 2015; Martynoga et al., 2005) and reduced expression of dorsal markers (Figure 1C), indicating their ventral NPC fates. Immunostaining of Mut NPCs at D20 illustrated a marked increase in ventral NKX2-1$^+$ and DLX1/2$^+$ NPCs, accompanied by a dramatic reduction in dorsal PAX6$^+$ and NGN1$^+$ NPCs (Figures 1D, 1E, S1K, and S1L). It was noteworthy that dorsal NPC makers did not colocalize with ventral NPC markers in either WT or Mut NPCs at D20 (Figures 1D and S1K). These differential gene expression patterns were reproducible among different cell lines (Figure S1M). These data indicate that the NR2F1-R112K mutation promotes the production of ventral NPCs and inhibits dorsal NPC differentiation fate, leading to the dysregulated specification of dorsal-ventral NPCs.

Because ventral NPCs give rise to the majority of cortical inhibitory neurons (Wonders and Anderson, 2006), we investigated whether Mut hESCs preferentially differentiate into inhibitory neurons at D45. qPCR analyses showed that the transcript levels of inhibitory neuron or synapse markers (*VGAT*, *GAD1*, *GAD2*, and *Gephyrin*) (Choii and Ko, 2015; Mariani et al., 2015; Tamamaki et al., 2003) were increased in Mut neurons at D45, whereas the RNA expression of excitatory neuron or synapse markers (*VGLUT1*, *VGLUT2*, *TBR1*, and *Homer1*) (Brakeman et al., 1997; Fremeau et al., 2001; Mariani et al., 2015) showed a significant decrease, compared with their WT counterparts (Figure 1F). These changes were confirmed by quantification of excitatory VGLUT1$^+$ or inhibitory VGAT$^+$ neurons at D45 (Figures 1G–1I). Thus, the overproduction of inhibitory neurons and the underproduction of excitatory neurons lead to an imbalance between the numbers of excitatory and inhibitory neurons. Furthermore, quantification of synaptic puncta revealed a decrease in excitatory Homer1$^+$ puncta and a significant increase in inhibitory Gephyrin$^+$ puncta in Mut neurons (Figures 1J–1L), suggesting an increase in the number of inhibitory synapses and a decrease in the number of excitatory synapses.

To rule out off-target possibilities, we generated mutation-reversed hESCs (Rev hESCs), in which the NR2F1-R112K mutation was corrected and a synonymous mutation of *NR2F1* gene (GRCh38.p12; chr5:93585371G>A; c.348G>A; p.R116R) was introduced simultaneously to distinguish Rev hESCs from WT hESCs (Figure S2A). We found that the altered neuron differentiation was restored in Rev hESCs at both D20 and D45 (Figures S2B–S2H), supporting the notion that the NR2F1-R112K mutation is entirely responsible for the altered neuron differentiation.

To examine the electrophysiological activities of WT and Mut neurons, we performed a patch-clamp recording on neurons at day 65 after neuron differentiation (D65), when neurons generated from hESCs *in vitro* show a steadily electrophysiological maturation (Johnson et al., 2007). WT and Mut neurons exhibited equivalent electrical excitability (Figures 1M and 1N). We also investigated the miniature synaptic currents in some neurons (Figure 1O). The amplitudes and frequencies of miniature excitatory postsynaptic currents (mEPSCs) of Mut neurons were lower than those of WT neurons (Figure 1P). However, the frequencies of miniature inhibitory postsynaptic currents (mIPSCs) of Mut neurons were higher, whereas the amplitudes of mIPSCs displayed no significant changes (Figure 1Q). Taken together, these data indicate that the NR2F1-R112K mutation promotes the production of inhibitory neurons and reduces the production of excitatory neurons, leading to the E/I imbalance.

## The Hedgehog Signaling Pathway Is Aberrantly Activated in Mut NPCs

To investigate the molecular mechanisms underlying the dysregulated specification of dorsal-ventral NPCs, we analyzed the global transcriptome of WT and Mut NPCs at D20 with two biological replicates (Figure 2A). The limited line-to-line variability revealed by correlation analysis indicates the high reproducibility of our samples (Figure S3A). First, we compared the transcriptome of either WT or Mut NPCs with BrainSpan's atlas (Kang et al., 2011) and found that both WT and Mut NPCs best reflected early embryonic human brain development (8–9 weeks postconception [8–9_pcw]) (Figure 2B). This indicates that the NR2F1-R112K mutation did not accelerate or delay the neuron-differentiation process. With regard to regional specification, the transcriptome of WT NPCs was similar to that of human dorsal telencephalon (including cerebral cortex and hippocampus) (Figure 2B), which was close to that of previous studies (Eiraku et al., 2008; Li et al., 2017a; Mariani et al., 2012). In contrast, the transcriptome of Mut NPCs was most similar to that of human ventral telencephalon, especially to that of medial ganglionic eminence (MGE), caudal ganglionic eminence (CGE), and lateral ganglionic eminence (LGE) (Figure 2B). These results confirm that Mut hESCs adopt the differentiation preference into ventral telencephalic NPCs. Next, both WT and Mut NPCs transcriptome were analyzed by differential gene expression (DEG) analysis (Figure 2C). Gene Ontology (GO) terms annotated by inhibitory neuron differentiation (including *DLX1*, *DLX2*, *ASCL1*, *LHX8*, *ISL1*, *NKX2-1*, and *FOXG1*) were enriched in Mut NPCs (Figure 2C). In contrast, many transcription factors (such as *PAX6*, *NGN1*, *NGN2*, *EMX1*, *EMX2*, *TBR2*, and *TBR1*) ensuring excitatory neuron differentiation showed dramatic downregulation in Mut NPCs (Figure 2C). Intriguingly, the genes related to

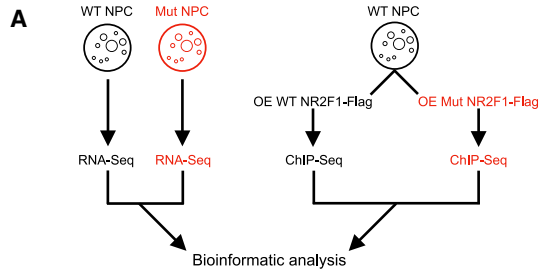


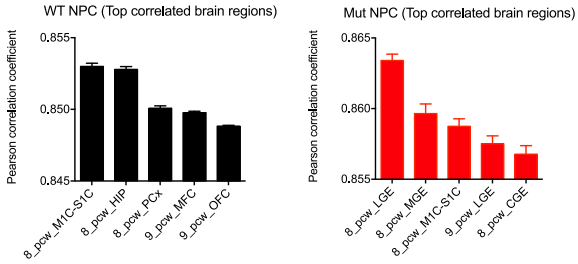


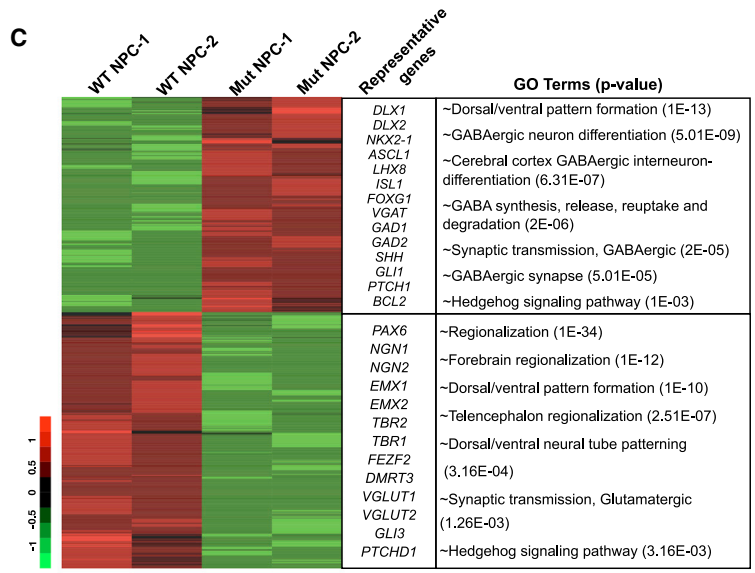


D

| PATHWAY | WT NPC | Mut NPC |
|---|---|---|
| TGFB_A | 16.65 | 6.65 |
| TGFB_I | -14.09 | -10.59 |
| BMP_A | 12.64 | 1.77 |
| BMP_I | 0.00 | -0.08 |
| HEDGEHOG_A | 0.07 | 40.39 |
| HEDGEHOG_I | -16.03 | -1.47 |
| FGF_A | 3.48 | 3.34 |
| FGF_I | -2.73 | -2.65 |
| HIPPO_A | 10.19 | 0.07 |
| HIPPO_I | -4.47 | -3.27 |
| NODAL_A | 4.94 | 2.26 |
| NODAL_I | -6.71 | -1.59 |
| NOTCH_A | 8.89 | 4.77 |
| NOTCH_I | -4.96 | -6.93 |
| WNT_A | 1.59 | 1.47 |
| WNT_I | -1.85 | -0.07 |

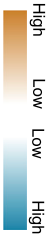


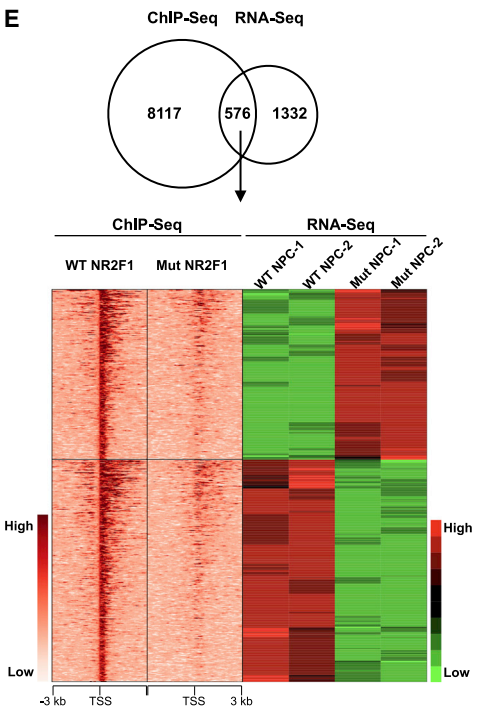


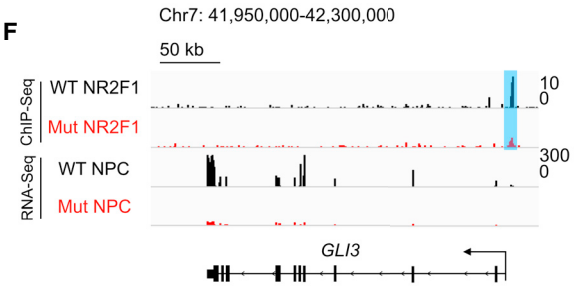


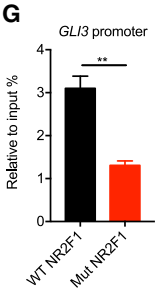


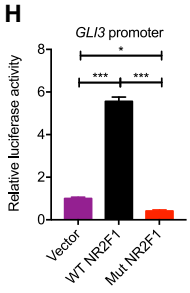


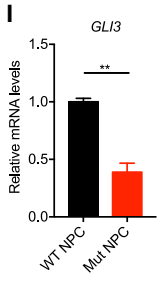


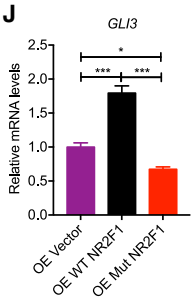


*(legend on next page)*

inhibitory (γ-aminobutyric acid [GABAergic]) synaptic transmission were highly expressed in Mut NPCs, whereas the excitatory (glutamatergic) synaptic transmission-associated genes were downregulated (Figures 2C and S3B). These results further illustrate that Mut hESCs have a preference toward differentiating into ventral NPCs and imply their inhibitory neuron fate.

Surprisingly, signaling pathway enrichment analysis unveiled an aberrant activation of the Hedgehog pathway in Mut NPCs (Figure 2D), indicated by upregulation of Hedgehog target genes or activators (*GLI1*, *SHH*, and *PTCH1*) (Katoh and Katoh, 2009; Lee et al., 1997; Sheng et al., 2004) and downregulation of Hedgehog pathway repressors (*GLI3* and *GPR161*) (Motoyama and Aoto, 2006; Mukhopadhyay et al., 2013) in the transcriptome of Mut NPCs (Figures 2C and S3B). Hedgehog pathway activation in Mut NPCs was further confirmed by gene-set enrichment analysis (GSEA) and the Gli-luciferase reporter assay (Figures S3C–S3E). Comparison of our DEGs with an independent study (DeRosa et al., 2018) indicates that both the Hedgehog pathway activation and the dysregulated dorsal-ventral specification are implicated in ASD patients' induced pluripotent stem cell (iPSC)-derived NPCs (Figure S3F).

To further investigate the underlying mechanism of the aberrantly activated Hedgehog signaling pathway, chromatic immunoprecipitation sequencing (ChIP-seq) was performed in H9 hESCs-derived NPCs overexpressing an equal amount of pcDNA3.1$^{+}$-WT/Mut NR2F1-Flag plasmids with two biological replicates (Figures 2A and S3G). The DNA-protein complex was precipitated by Flag beads. The replicates were merged because of the narrow variations (Figure S3H). When compared with WT NR2F1, Mut NR2F1 showed decreased enrichment in the regions within the transcription start site (TSS) ± 3,000 bp (Figure S3I), implying the reduced DNA-binding activity of Mut NR2F1. To investigate whether NR2F1 binding affected the expression of target genes, we integrated ChIP-seq data with DEGs (Figure 2E). Among 576 differentially expressed genes bound by WT or Mut NR2F1, several Hedgehog pathway regulators (*GLI3*, *GAS1*, *WNT9A*, *PTCH1*, *FGF9*, *SALL3*, and *WNT7B*) were identified (Table S2). *GLI3* presented the highest peak score among these regulators and was a major Hedgehog pathway repressor in telencephalic development (Motoyama and Aoto, 2006). Reduced enrichment of Mut NR2F1 in the promoter region of *GLI3* (compared with WT NR2F1) was identified in ChIP-seq analysis, ChIP-qPCR and luciferase assays (Figures 2F–2H). Decreased expression of *GLI3* in Mut NPCs was observed in RNA-seq analysis and the qPCR assay (Figures 2F and 2I). Moreover, we found that overexpression of WT NR2F1 in the H9 hESCs-derived NPCs increased the *GLI3* transcript levels, whereas overexpression of Mut NR2F1 led to the downregulation of *GLI3* (Figure 2J). This suggests that WT NR2F1 positively regulates *GLI3*, and that the regulation is abolished by the NR2F1-R112K mutation. We also found that Mut NR2F1 displayed decreased enrichment in the promoter or enhancer regions of *GLI1*, *PTCH1*, and *SHH* (Figures S3J–S3N) and that these Hedgehog target genes or activators were upregulated in Mut NPCs at D20 (Figure S3O). These differentially expressed genes indicate the activation of Hedgehog pathway, and it raises the hypothesis that the aberrantly activated Hedgehog signaling pathway accounts for the imbalance of excitatory/inhibitory neuron differentiation.

## Hedgehog Pathway Activation Is Mainly Responsible for the Altered Neuron Differentiation

To test this hypothesis, cyclopamine, an antagonist of the Hedgehog pathway (2 μM) (Chen et al., 2002), was administrated from D10 to D20 during neuron differentiation, following previous studies (Li et al., 2009; Srikanth et al., 2015) (Figure 3A). This treatment led to decreased Hedgehog pathway activities in Mut NPCs, but not WT NPCs, determined by the Gli-luciferase reporter assay (Figure 3B). Importantly, the expression levels of ventral NPC markers (*DLX1*, *DLX2*, *NKX2-1*, and *ASCL1*) at D20 were downregulated, whereas dorsal NPC markers (*NGN1*, *NGN2*, *PAX6*, and *TBR2*) were upregulated in the cyclopamine-treated Mut cells (Figures 3C–3E). Furthermore, at D45, inhibitory neuron or synapse

**Figure 2. The Hedgehog Signaling Pathway Is Aberrantly Activated in Mut NPCs**

(A) Diagram of sample preparations for RNA-seq and ChIP-seq.

(B) Transcriptome correlation between WT or Mut NPCs at D20 and human brain samples from BrainSpan's database. The left or right column shows the top five correlated brain regions of WT or Mut NPCs, respectively. 8/9_pcw, 8/9 post-conception weeks; M1C, primary motor cortex; S1C, primary somatosensory cortex; HIP, hippocampus; PCx, parietal cortex; MFC, medial frontal cortex; OFC, orbitofrontal cortex; LGE, lateral ganglionic eminence; MGE, medial ganglionic eminence; CGE, caudal ganglionic eminence.

(C) The heatmap shows the differentially expressed genes (DEGs) between WT and Mut NPCs at D20. Representative genes and Gene Ontology (GO) terms are shown in the right column.

(D) Analysis of signaling pathways involved in embryonic brain development. Brown or blue indicates an activated enrichment or an inhibited enrichment, respectively (I, inhibit; A, activate). The value in each cell represents $\log_{10}$ (false discovery rate [FDR]), and the brown or blue border indicates significant enrichment (FDR < 0.01).

(E) Venn diagrams summarizing the integrating WT and/or Mut NR2F1-bound genes (ChIP-seq data) with DEGs (RNA-seq data) (top). The heatmaps of expression patterns of these overlapped genes and the corresponding ChIP-seq signals generated by WT/Mut NR2F1 (bottom).

(F) Genome browser snapshot of the NR2F1 enrichment in the *GLI3* locus and the expression changes of *GLI3*. The blue rectangle indicates the enrichment regions of NR2F1.

(G and H) Verification of NR2F1 enrichment in the promoter region of the *GLI3* gene by ChIP-qPCR assay (G) and luciferase assay (H). The expression is normalized to negative control levels (G) and the empty vector (H).

(I) Verification of the *GLI3* expression in WT and Mut NPCs at D20 by qPCR assay. The expression is normalized to GAPDH and WT levels.

(J) The *GLI3* expression in H9 hESCs-derived NPCs by overexpressing an equal amount of empty vector or pcDNA3.1$^{+}$-WT/Mut NR2F1. The expression is normalized to GAPDH and to empty vector levels.

Data are presented as means ± SEM; n represents separate experiments. WT, n = 3 (G)–(J); Mut, n = 3 (G)–(J); vector, n = 3 (H) and (J); Student's t test analysis was used in (G) and (I). One-way ANOVA analysis with Tukey's test was used in (H) and (J).

See also Figure S3 and Table S2.

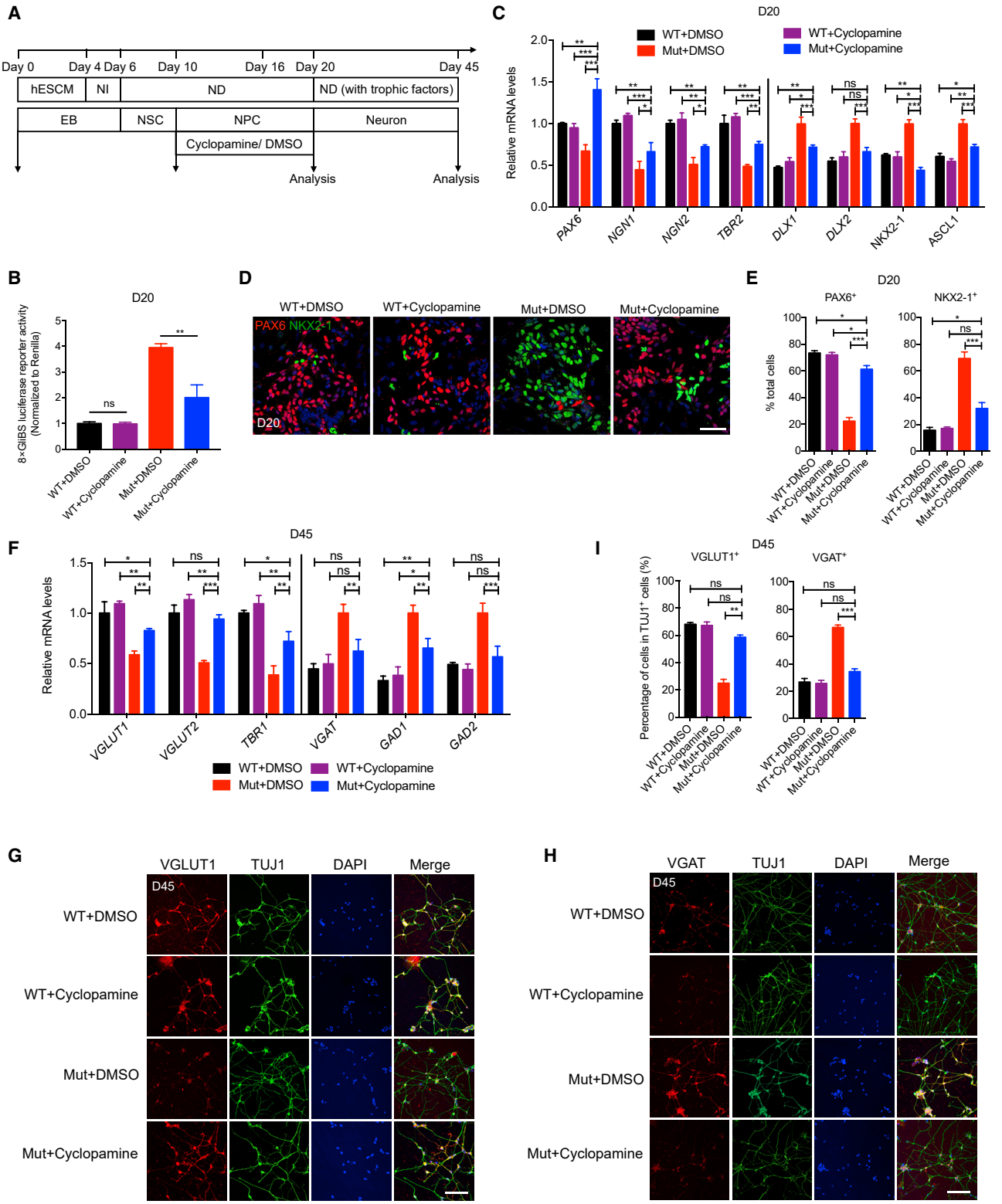


**Figure 3. Antagonist of Hedgehog Pathway Could Mainly Rescue the Altered Neuron Differentiation**

(A) Schematic diagram of cyclopamine treatment. Treatment of DMSO or cyclopamine (2 μM) ranges from D10 to D20 in neuron-differentiation process.

(B) Hedgehog pathway activity measured by the Gli-luciferase reporter assays in WT or Mut NPCs at D20 with prior DMSO or cyclopamine treatment. 8 × GliBS, 8 × Gli binding sites-containing luciferase reporter.

*(legend continued on next page)*

markers were downregulated, whereas excitatory neuron or synapse markers were upregulated in Mut cells with cyclopamine treatment (Figures 3F–3I). These data show that cyclopamine treatment can mainly rescue the altered neuron differentiation at both D20 and D45 and confirm the hypothesis that Hedgehog pathway activation in Mut cells mainly accounts for the imbalance of excitatory/inhibitory neuron differentiation.

## The Imbalance of Excitatory/Inhibitory Neurons Is Observed in the Primary Somatosensory Cortex of Nr2f1$^{+/m}$ Mice

Considering that the *Nr2f1* gene is identified as a regulator of cortical patterning in the sensory area during mouse brain development (Armentano et al., 2007) and that the primary somatosensory cortex is frequently influenced in many ASD mouse models (Collignon et al., 2013; Marco et al., 2012), we asked whether the altered neuron differentiation could be recapitulated in the primary somatosensory cortex using a mouse model.

To generate an *in vivo* model, we introduced the corresponding point mutation of *Nr2f1* gene (GRCm38.p6; chr13:78198248G>A; c.326G>A; p.R109K) into fertilized mouse eggs. After a series of crossings, heterozygous point-mutation mice (Nr2f1$^{+/m}$ [+/m]) and WT mice (Nr2f1$^{+/+}$ [+/+]) were obtained, but homozygous point-mutation mice (Nr2f1$^{m/m}$ [m/m]) were not (Figure S4A; Table S3). We first examined whether the point mutation of the mouse *Nr2f1* gene affected the dorsal-ventral telencephalic specification and Hedgehog pathway activity at embryonic day 12.5 (E12.5). Similar to observations in Mut NPCs, we found reduced expression of dorsal NPC markers (*Pax6*, *Ngn1*, and *Emx1*) and increased expression of ventral NPC markers (*Nkx2-1* and *Gsx1*), as well as elevated Hedgehog pathway activity (revealed by upregulation of *Shh* and *Gli1* and downregulation of *Gli3*), in the whole brain of Nr2f1$^{+/m}$ mice embryos, compared with Nr2f1$^{+/+}$ embryos (Figure S4B). Importantly, at 2 months old (2M), Nr2f1$^{+/m}$ mice had decreased numbers of Cux1$^{+}$ and Ctip2$^{+}$ excitatory projection neurons (Leone et al., 2008; Nieto et al., 2004) and increased numbers of Gad1$^{+}$, PV$^{+}$, and SST$^{+}$ inhibitory interneurons (Tamamaki et al., 2003; Wonders and Anderson, 2006) in the primary somatosensory cortex, compared with their Nr2f1$^{+/+}$ littermates (Figures 4A–4F and 4H). Furthermore, Nr2f1$^{+/m}$;Gad1-GFP mice were generated (Tamamaki et al., 2003), and the number of Gad1-GFP$^{+}$ neurons was also increased, compared with Nr2f1$^{+/+}$;Gad1-GFP mice (Figures 4G and 4H). These data indicate that there is an overproduction of inhibitory neurons and an underproduction of excitatory neurons in the primary somatosensory cortex of Nr2f1$^{+/m}$ mice.

Additionally, the number of excitatory and inhibitory neurons in the prefrontal cortex (PFC), which is also considered to be affected in neurodevelopmental disorders (Courchesne et al., 2011; Kemper and Bauman, 1998), was investigated. The number of inhibitory Gad1$^{+}$ neurons was increased in Nr2f1$^{+/m}$ mice (Figure S4C), whereas the number of excitatory Ctip2$^{+}$ or GluR2$^{+}$ neurons was mainly unchanged (Figure S4D). The discrepancy of excitatory projection neuron phenotypes between primary somatosensory cortex and PFC may originate from the fact that the expression of *Nr2f1* gene was high in the sensory cortex but low in the frontal cortex (Armentano et al., 2007). Thus, we focused on analysis of the primary somatosensory cortex in this study.

We also found electrophysiological evidence for the increased inhibitory phenotypes in 1–2-month-old Nr2f1$^{+/m}$ mice. Although the action potentials of primary somatosensory cortex neurons in Nr2f1$^{+/+}$ and Nr2f1$^{+/m}$ mice displayed no significant differences (Figures 4I and 4J), the amplitudes and frequencies of mEPSCs in Nr2f1$^{+/m}$ mice were reduced (Figures 4K and 4M), whereas the amplitudes and frequencies of mIPSCs were increased (Figures 4L and 4N). Taken together, these data indicate that there is an imbalance of excitatory/inhibitory neurons in the primary somatosensory cortex of Nr2f1$^{+/m}$ mice.

## Nr2f1$^{+/m}$ Mice Display Impaired Social Interactions, Repetitive Behaviors, Learning and Memory Deficits, and Anxiety

Because the imbalance of excitatory/inhibitory neurons may underlie behavioral deficits in many models for neurodevelopmental disorders (Gogolla et al., 2009; Rubenstein, 2010; Yizhar et al., 2011), Nr2f1$^{+/+}$ and Nr2f1$^{+/m}$ male mice generated by *in vitro* fertilization (IVF) at 2M were examined using a series of behavioral tests. In the social affiliation and sociability test, Nr2f1$^{+/+}$ mouse displayed a preference for an age-matched male mouse (N) to an inanimate object (O), whereas the preference was undetectable in Nr2f1$^{+/m}$ mouse (Figures 5A–5D). In the social memory and novelty test, the preference for a novel mouse (N) to the familiar mouse (F) was not identified in Nr2f1$^{+/m}$ mouse (Figures 5E–5H). These abnormalities measured in the three-chamber test indicate the impaired social interactions of Nr2f1$^{+/m}$ mouse. Compared with the Nr2f1$^{+/+}$ mouse, the Nr2f1$^{+/m}$ mouse spent more time in self-grooming, implying more repetitive behaviors (Figures 5I and S5A; Videos S1). The Y-maze test has been used to evaluate both repetitive behaviors and learning and memory abilities (Bruto et al., 1984; Conrad et al., 1997; Markram et al., 2008). Spontaneous alternations measured in the Y-maze test were decreased in the Nr2f1$^{+/m}$ mouse (Figure 5J), suggesting abnormal repetitive behaviors and impaired learning and memory abilities. Furthermore, anxious behaviors were observed in the Nr2f1$^{+/m}$ mouse by using the dark-light emergency test (Figure 5K), the elevated plus maze test (Figure 5L), and the open-field test (Figures 5M and 5N). Finally,

(C) Relative RNA expression levels of dorsal (*PAX6*, *NGN1*, *NGN2*, and *TBR2*) and ventral (*DLX1*, *DLX2*, *NKX2*-1, and *ASCL1*) NPC markers at D20. The expression is normalized to GAPDH and WT+DMSO or Mut+DMSO levels.

(D and E) Immunostaining (D) and quantification (E) of dorsal (PAX6) and ventral (NKX2-1) NPC markers at D20.

(F) Relative RNA expression levels of excitatory (*VGLUT1*, *VGLUT2*, and *TBR1*) and inhibitory (*VGAT*, *GAD1*, and *GAD2*) neuron or synapse markers at D45. The expression is normalized to GAPDH and WT+DMSO or Mut+DMSO levels.

(G–I) Immunostaining (G) and quantification (I) of excitatory (VGLUT1) or inhibitory (VGAT) (H and I) neuron or synapse markers at D45.

Data are presented as means ± SEM; n represents three separate experiments of neuron differentiation within the same condition. Scale bar, 30 μm (D) and 50 μm (G and H). One-way ANOVA analysis with Tukey's test was used in (B), (C), (E), (F), and (I).

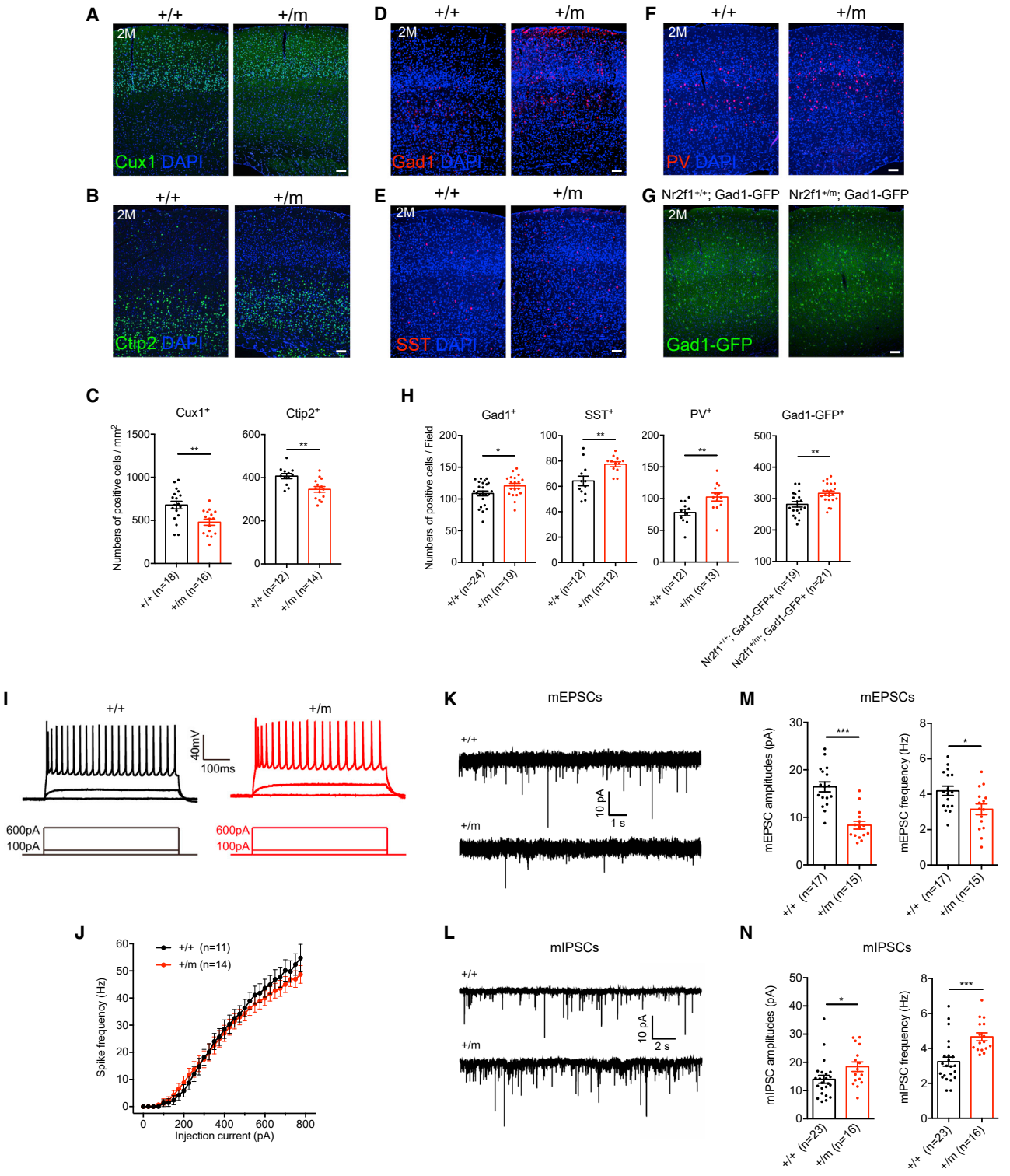


**Figure 4. The Imbalance of Excitatory/Inhibitory Neurons Is Observed in the Primary Somatosensory Cortex of Nr2f1$^{+/m}$ Mice**

(A–C) Immunostaining (A) and quantification (C) of excitatory Cux1 and Ctip2 (B and C) neuron markers at 2M. +/+, Nr2f1$^{+/+}$; +/m, Nr2f1$^{+/m}$. Scale bar, 200 μm.

(D–H) Immunostaining (D) and quantification (H) of inhibitory Gad1, SST (E and H), PV (F and H), and Gad1-GFP (G and H) neuron markers at 2M. +/+, Nr2f1$^{+/+}$; +/m, Nr2f1$^{+/m}$. Scale bar, 200 μm.

(I–N) Electrophysiological recordings are conducted by using 1–2-month-old mice.

*(legend continued on next page)*

the rotarod test data (Figure 5O) excluded motor impairment for both Nr2f1$^{+/m}$ and Nr2f1$^{+/+}$ mice. These behavioral tests clearly show that the Nr2f1$^{+/m}$ mouse has impaired social interactions, repetitive behaviors, learning and memory deficits, and anxiety. Similarly, many of these behavioral deficits were identified in Nr2f1$^{+/m}$ female mice (Figures S5B–S5G). In addition, naturally conceived Nr2f1$^{+/m}$ mice were also generated, and they displayed similar behavioral deficits as IVF-generated Nr2f1$^{+/m}$ mice (Figures S5H–S5S). Together, these behaviors phenocopy the symptoms of neurodevelopmental disorders, including ASD, intellectual disability, and obsessive-compulsive behaviors, which are observed in the patient carrying the NR2F1-R112K mutation (Bosch et al., 2014).

### Ginkgolide A Treatment Partially Alleviates Behavioral Deficits of Nr2f1$^{+/m}$ Mice

Given the possibility of the increased inhibitory synaptic transmission in determining behavioral deficits, we asked whether antagonizing the inhibitory synaptic transmission could alleviate behavioral deficits of Nr2f1$^{+/m}$ mice. Ginkgolide A, an extract from *Ginkgo biloba*, is a known antagonist of inhibitory synaptic transmission and has been used to alleviate anxiety (Huang et al., 2004; Kuribara et al., 2003). Its homolog (bilobalide) can antagonize the inhibitory synaptic transmission in mouse models for Down syndrome (Fernandez et al., 2007). Oral gavage of ginkgolide A at 2 mg/kg (a non-epileptic dose) (Kuribara et al., 2003) was conducted daily for 1 week (from the age of 7 weeks) in both Nr2f1$^{+/+}$ and Nr2f1$^{+/m}$ mice, and behaviors were tested at 8 weeks of age (Figure 6A). Impaired social interactions measured in the three-chamber test were principally rescued in Nr2f1$^{+/m}$ mice with ginkgolide A treatment (Figures 6B–6E). Ginkgolide A partially reduced the repetitive behaviors of Nr2f1$^{+/m}$ mice (Figure 6F) in the self-grooming test, but not in the Y-maze test (Figure 6G), indicating that the impaired learning and memory ability could not be rescued by ginkgolide A. Consistent with the previous study (Kuribara et al., 2003), ginkgolide-A-treated Nr2f1$^{+/m}$ mice spent more time in the open arms during the elevated plus maze test (Figure 6H), indicating a reduction in anxious behaviors. These data suggest that ginkgolide A treatment partially alleviates impaired social interactions, repetitive behaviors, and anxiety in Nr2f1$^{+/m}$ mice.

To further investigate the mechanism underlying this alleviation, electrophysiological tests of both Nr2f1$^{+/+}$ and Nr2f1$^{+/m}$ mice were performed at 8 weeks of age after 1 week of drug administration (Figures 6I and 6K). The frequencies of mIPSCs of Nr2f1$^{+/m}$ mice were lower after ginkgolide A treatment, whereas the frequencies and amplitudes of mEPSCs and the amplitudes of mIPSCs of Nr2f1$^{+/m}$ mice displayed no significant changes (Figures 6J and 6L). These data indicate that the amelioration by ginkgolide A treatment was partially mediated by reversing the frequencies of mIPSCs.

### Ginkgolide A Treatment Has No Detectable Long-Term Improvement on Behavioral Deficits of Nr2f1$^{+/m}$ Mice

To investigate whether ginkgolide A treatment causes long-term improvement in behavioral deficits, we performed several behavioral tests on those mice that were administered ginkgolide A. At 12 weeks after the original ginkgolide A treatment, impaired social interactions were detected in both vehicle- and ginkgolide-A-treated Nr2f1$^{+/m}$ mice, implying that ginkgolide A has no long-term improvement effect in the three-chamber test (Figures S6A–S6D). Similarly, no improvement was observed in the Y-maze or self-grooming test (Figures S6E and S6F). To further evaluate the effect of ginkgolide A on learning and memory deficits, an additional 2-object novel object recognition test was performed (Bevins and Besheer, 2006). We found that learning and memory deficits existed in both vehicle- and ginkgolide-A-treated Nr2f1$^{+/m}$ mice (Figures S6G and S6H), implying that Nr2f1$^{+/m}$ mice had impaired learning and memory ability and that ginkgolide A had minimal long-term effects on learning and memory deficits. To test the short-term effect of Ginkgolide A on the 2-object novel object recognition test, we performed another 1-week ginkgolide A administration on those mice. No improvement in the 2-object novel object recognition test was detected in ginkgolide-A-treated Nr2f1$^{+/m}$ mice (Figures S6I and S6J), suggesting that ginkgolide A had no effect on learning and memory ability. Thus, ginkgolide A treatment has no detectable long-term improvement on the behavioral deficits of Nr2f1$^{+/m}$ mice.

## DISCUSSION

Here, we present a framework for establishing a bridge between embryonic neuron differentiation and human neurodevelopmental disorders, such as ASD. In our study, Mut hESCs exhibited overproduction of ventral NPCs and underproduction of dorsal NPCs, leading to an E/I imbalance that was restored in Rev hESCs (Figures 1 and S2). We showed that Hedgehog pathway activation in Mut cells was mainly responsible for the imbalance of excitatory/inhibitory neuron differentiation (Figures 2 and 3). Furthermore, Nr2f1$^{+/m}$ mouse displayed a similar E/I imbalance in the primary somatosensory cortex (Figure 4) and exhibited behavioral deficits of neurodevelopmental disorders, including ASD (Figure 5). These behavioral deficits were partially alleviated by antagonizing the increased inhibitory synaptic transmission (Figure 6). These data confirm the causal relationship between the NR2F1-R112K mutation and ASD features and imply that

(I) Example recording traces depicting the action potential firing of neurons in response to the step depolarizing currents (500-ms duration).
(J) The plot of evoked spike rates versus the current magnitudes (input-output curve) neurons.
(K–N) Representative recordings (K) and quantification (M) of miniature excitatory postsynaptic currents (mEPSCs) and miniature inhibitory postsynaptic currents (mIPSCs) (L and N).
Data are presented as means ± SEM; n represents the numbers of brain slices (C and H), 2–5 slices/mouse; n represents the numbers of recorded neurons (J, M, and N). Data are collected from several Nr2f1$^{+/+}$ mice, five in (C) and (H); four in (J) and (M); and three in (N); and in Nr2f1$^{+/m}$ mice, four in (C), (H), (J), and (M); and five in (N). Data are collected from five Nr2f1$^{+/+}$;Gad1-GFP mice and from five Nr2f1$^{+/m}$;Gad1-GFP mice (C); Student's t test analysis is used in (C), (H), (J), (M), and (N).
See also Figure S4 and Table S3.

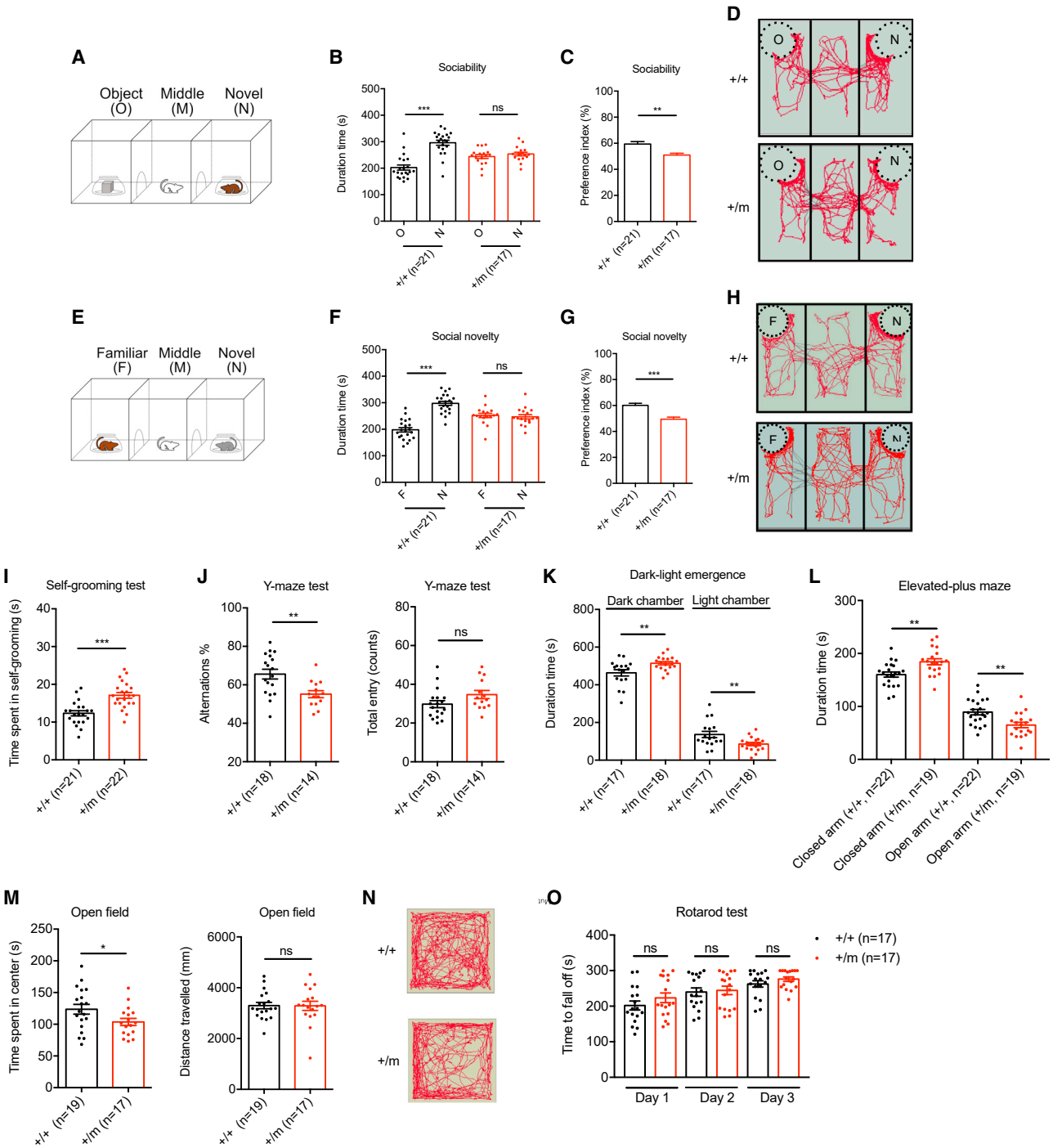


**Figure 5. Nr2f1$^{+/m}$ Mice Display Impaired Social Interactions, Repetitive Behaviors, Learning and Memory Deficits, and Anxiety**

(A) Schematic diagram of the social affiliation and sociability test in the three-chamber test.

(B and C) Comparison of time spent in interaction (B) and preference index (C) for novel mouse in the social affiliation and sociability test. O, object; N, novel mouse.

(D) Representative trajectories of Nr2f1$^{+/+}$ and Nr2f1$^{+/m}$ mice in the social affiliation and sociability test.

(E) Schematic diagram of the social memory and novelty test in the three-chamber test.

(F and G) Comparison of time spent in interaction (F) and preference index (G) for novel mouse in the social memory and novelty test. N, novel mouse; F, familiar mouse.

(H) The representative trajectories of Nr2f1$^{+/+}$ and Nr2f1$^{+/m}$ mice in the social memory and novelty test.

*(legend continued on next page)*

the point mutation in the *NR2F1* gene is a molecule signature of neurodevelopmental disorders, especially ASD.

The imbalance between excitatory and inhibitory neurons was identified in our model. Specifically, the NR2F1-R112K mutation led to increased expression of inhibitory neuron or synapse markers and decreased excitatory markers in both hESCs-derived neurons and mouse brains (Figures 1 and 4). Furthermore, the electrophysiological imbalance of excitatory/inhibitory neurons was confirmed by differential changes in mEPSCs and mIPSCs (Figures 1 and 4). Interestingly, upregulation of inhibitory neuron or synapse markers (*GAD1*, *GAD2*, *VGAT*, *Gephyrin*, *SCN1A*, *GABRA1*, *GABRB3*, *GABBR1*, and *GLRA2*) and downregulation of excitatory markers (*VGLUT1*, *VGLUT2*, *GRID1*, *GRIK1*, *GRM3*, *RELN*, and *HOMER1*) were identified in the transcriptome of Mut NPCs (Figure S3), implying that differential expression of synaptic molecules was detectable in NPCs. Importantly, many of these synaptic markers were candidate genes for neurodevelopmental disorders, including ASD, and their dysregulated expression levels have been proven to cause the E/I imbalance and behavioral deficits (Banerjee et al., 2016; Buxbaum et al., 2002; Chang et al., 2011; Cossette et al., 2002; Fatemi et al., 2009; Han et al., 2012; Livide et al., 2015; Persico et al., 2001; Sandhu et al., 2014; Zhang et al., 2017). Thus, these data imply that the imbalance of excitatory/inhibitory neurons identified in our study closely correlates with neurodevelopmental disorders, especially ASD.

The increased inhibitory phenotypes described in our work have been observed in some ASD models (Adhya et al., 2019; Etherton et al., 2011; Lawrence et al., 2010; Mariani et al., 2015; Smith et al., 2011; Tabuchi et al., 2007). Our data suggest that the *NR2F1*-dependent imbalance of excitatory/inhibitory neurons leads to behavioral deficits (Figure 5), confirmed by the fact that antagonizing the increased inhibitory synaptic transmission partially alleviates the behavioral deficits of $Nr2f1^{+/m}$ mice (Figure 6). Meanwhile, the decreased inhibitory transmission has been identified in other ASD models (Rubenstein and Merzenich, 2003), and some agonists of GABAergic receptors have been shown to improve behavioral deficits (Han et al., 2012, 2014). These divergent results indicate that restoration of the balance between excitatory and inhibitory neurons, which should be considered on a case-by-case basis, is important in the treatment of neurodevelopmental disorders, including ASD. Our study may enlighten personalized medicine.

Ginkgolide A is extracted from *Ginkgo biloba* and has previously been shown to antagonize inhibitory transmitter receptors (Huang et al., 2004). It has been revealed that ginkgolide A has an anxiolytic-like effect but does not have a pronounced tendency to produce benzodiazepine-like side effects (Kuribara et al., 2003). However, the effects of ginkgolide A treatment on behavioral deficits of neurodevelopmental disorders, such as ASD, are mainly unknown. We showed that ginkgolide A treatment ameliorated impaired social interactions, repetitive behaviors, and anxious behaviors in $Nr2f1^{+/m}$ mice, mainly by reversing the frequencies of mIPSCs (Figure 6). However, impaired learning and memory ability, which was detected in both the Y-maze test and the 2-object novel object recognition test, could not be alleviated by ginkgolide A treatment (Figures 6 and S6). Lasting improvement of symptoms after ginkgolide A treatment was not observed (Figure S6), suggesting that the treatment should be applied at regular intervals. In addition, it has been reported that ginkgolide A may reduce inflammatory responses (Li et al., 2017b; Zhao et al., 2015). Further investigations are warranted to explore whether the anti-inflammatory effects of ginkgolide A contribute to alleviating behavioral deficits of neurodevelopmental disorders.

It has been previously demonstrated that dorsal-ventral telencephalic patterning is critical for brain development (Campbell, 2003; Wilson and Rubenstein, 2000). However, it remains uncertain whether alterations in the specification of dorsal-ventral telencephalon could lead to neurodevelopmental disorders, including ASD. Our data showed that the E/I imbalance originated from the dysregulated specification of dorsal-ventral NPCs: upregulation of ventral NPC markers (*DLX1*, *DLX2*, *ASCL1*, *NKX2-1*, *ISL-1*, and *FOXG1*) and downregulation of dorsal markers (*PAX6*, *NGN1*, *NGN2*, *EMX1*, *TBR2*, and *TBR1*) in mutant cells (Figures 1 and 2). Furthermore, some of these expressed changes were recapitulated in the embryonic mutant mouse brain (Figure S4). Recent studies have revealed that abnormalities in the development of dorsal-ventral telencephalon are identified in other neurodevelopmental diseases, such as Down syndrome and Williams syndrome (Chakrabarti et al., 2010; Galaburda et al., 2001). In addition, some dorsal-ventral specification determinants (including *FOXG1*, *DLX1*, *DLX2*, *PAX6*, and *TBR1*) are identified as ASD candidates and show altered expression in the neurodevelopment of ASD models (Davis et al., 2008; De Rubeis et al., 2014; Kortüm et al., 2011; Liu et al., 2009; Mariani et al., 2015; O'Roak et al., 2012). Together, our results suggest a hypothesis that the common pathophysiology of many patients with ASD features may originate from abnormal development of dorsal-ventral telencephalon.

The Hedgehog pathway is essential for regulation of dorsal-ventral telencephalic specification because *Gli3* is required for dorsal telencephalic development, and *Shh* promotes ventral specification (Motoyama and Aoto, 2006; Rallu et al., 2002; Theil et al., 1999). However, little is known about the contribution of the Hedgehog pathway to the pathophysiology of neurodevelopmental disorders, such as ASD. In our study, we found that the

(I) Comparison of time spent in self-grooming.
(J) Comparison of spontaneous alternation percentage (left) and total entry (right) in the Y-maze test.
(K) Comparison of duration time in the dark or light chamber in the dark-light emergency test.
(L) Comparison of duration time in the open arms or closed arms in the elevated plus maze test.
(M) Comparison of duration time (left) in the central region and the total moving distance (right) in the open field test.
(N) The representative trajectories in the open field test.
(O) Comparison of duration time in the rotarod apparatus.
Data are presented as means ± SEM; n represents the numbers of tested mice. Student's t test analysis is used in (B), (C), (F), (G), (I)–(M), and (O).
See also Figure S5 and Video S1.

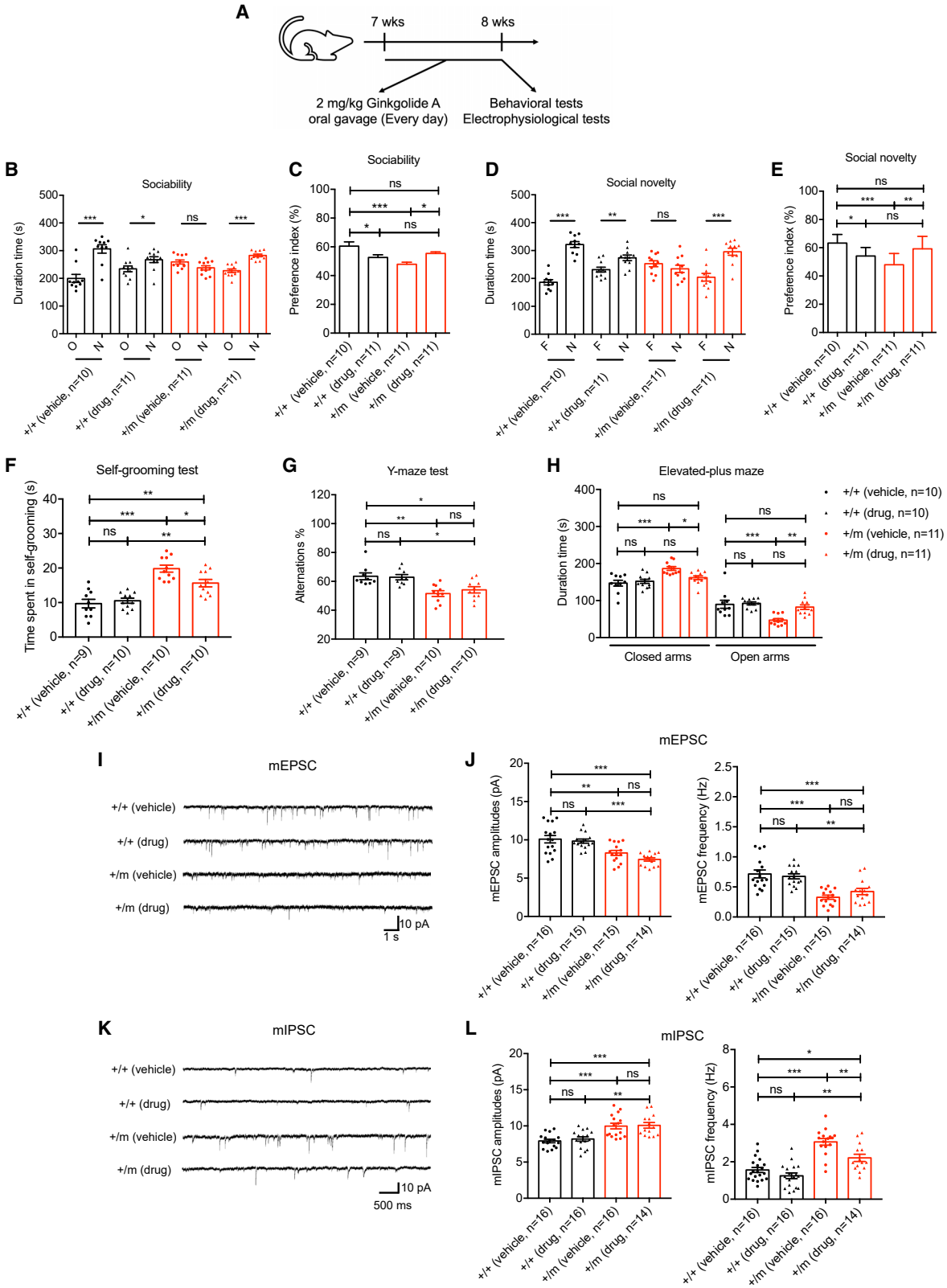


*(legend on next page)*

aberrantly activated Hedgehog signaling pathway in Mut NPCs was mostly responsible for the disturbed specification of dorsal-ventral NPCs and that dysregulation was partially restored with cyclopamine treatment (Figures 2 and 3). Specifically, Hedgehog pathway activation in Mut cells was revealed by upregulation of Hedgehog target genes or activators, including *SHH*, *GLI1*, and *PTCH1*, and decreased expression of *GLI3*, the major Hedgehog pathway repressor. The deficiency of *Gli3* in mouse has been shown to cause ventralized telencephalon development (Rallu et al., 2002), and some patients with Greig cephalopolysyndactyly syndrome (characterized by abnormal appearance and macrocephaly) carrying *GLI3* variants manifested ASD (Johnston et al., 2010; Siracusano et al., 2019). Genetic mutations or altered expression levels of Hedgehog pathway genes, such as *PTCHD1* and *BCL2*, have been identified in many neurological diseases, including intellectual disabilities and ASD (Fatemi and Halt, 2001; Noor et al., 2010). Consistent with this, altered expression levels of *PTCHD1* and *BCL2* were also observed in our RNA-seq analysis (Figure 2). Additionally, some ASD patients have higher serum concentrations of SHH protein (Al-Ayadhi, 2012). These studies suggest that the dysregulated Hedgehog signaling pathway could account for the pathophysiology in these patients.

Is there a common mechanism underlying neurodevelopmental disorders, such as ASD? Interestingly, when we integrated our RNA-seq data with that from another study (consisting of six ASD patients and five controls) (DeRosa et al., 2018), the GO terms annotated by dorsal-ventral neural tube patterning, telencephalon regionalization, and Hedgehog pathway activity were enriched in both our Mut NPCs and the ASD patients iPSCs-derived NPCs (Figure S3), suggesting that a unified mechanism may exist in these patients.

NR2F1 protein is not only a transcription factor but also a nuclear receptor. Similar to other nuclear receptors, NR2F1 acts as hetero- or homodimers and is translocated into the nucleus to regulate downstream targets (Cooney et al., 1992). The function of *Nr2f1* in mouse brain development has been extensively studied; however, the role of the *NR2F1* gene in human neurodevelopment and related disorders remains uncertain. Recent studies have identified several patients with NR2F1 mutations displaying ASD symptoms, and nearly half of those individuals carried heterozygous point mutations in the *NR2F1* gene (Chen et al., 2016). Moreover, those individuals with the heterozygous point mutant *NR2F1* gene have more severe symptoms compared with patients carrying heterozygous whole-gene deletions of *NR2F1* gene (Chen et al., 2016). In addition, the point mutation of the *NR2F1* gene led to decreased luciferase activity relative to the empty vector control in the *GLI3* promoter (Figure 2), which was similar to a previous publication (Chen et al., 2016). Moreover, our gain-of-function experiment showed that overexpression of Mut NR2F1 decreased the expression of *GLI3*, compared with the empty vector control (Figure 2). All the data above support the notion that the point mutation of *NR2F1* gene may act in a dominant-negative manner. However, we cannot exclude the possibility that a dosage-dependent effect may also contribute to some phenotypes observed in our study. The detailed mechanism awaits further investigations.

It has been demonstrated that BBSOAS is caused by *NR2F1* variants and that about 35% of patients with BBSOAS display ASD features. Additionally, recent studies have identified more NR2F1-mutant ASD patients (Chen et al., 2017; De Rubeis et al., 2014; Lim et al., 2017; Sanders et al., 2012), who did not meet diagnostic criteria for BBSOAS, suggesting that NR2F1 mutations might have a role in several neurodevelopmental disorders, including BBSOAS and ASD. Interestingly, the patient with the NR2F1-R112K mutation also displayed obsessive-compulsive disorder (an anxiety-related disorder), which was not identified in other patients with BBSOAS (Bosch et al., 2014; Chen et al., 2016). This implies that the R112K mutation may work in a unique manner. In addition, many patients with ASD also exhibit other symptoms, including intellectual disability and anxiety. Taken together, more cases should be collected in the future to clarify the role of NR2F1 mutations in the pathogenesis of neurodevelopmental disorders.

Although the NR2F1-R112K mutation is a rare mutation and, therefore, represents a limited population of patients, the results presented here suggest that a shared pathophysiological mechanism for neurodevelopmental disorders, especially ASD, may exist. Elucidation of this mechanism may benefit diagnosis and personalized treatment.

## STAR★METHODS

Detailed methods are provided in the online version of this paper and include the following:

- KEY RESOURCES TABLE
- LEAD CONTACT AND MATERIALS AVAILABILITY
- EXPERIMENTAL MODEL AND SUBJECT DETAILS
  - Mouse strains
  - Cell culture

**Figure 6. Ginkgolide A Treatment Partially Alleviates Behavioral Deficits of Nr2f1$^{+/m}$ Mice**

(A) Schematic diagram of administration of ginkgolide A. 7/8 wks, 7–8 weeks old.

(B and C) Comparison of time spent in interaction (B) and preference index (C) for novel mice in the social affiliation and sociability test. O, object; N, novel mouse.

(D and E) Comparison of time spent in interaction (D) and preference index (E) for novel mice in the social memory and novelty test. N, novel mouse; F, familiar mouse.

(F) Comparison of time spent in self-grooming.

(G) Comparison of spontaneous alternation percentage in the Y-maze test.

(H) Comparison of duration time in the open arms or closed arms in the elevated plus maze test.

(I–L) Representative recordings (I) and quantification (J) of the mEPSCs and recordings (K) and quantification (L) of mIPSCs from neurons in the primary somatosensory cortex of Nr2f1$^{+/+}$ and Nr2f1$^{+/m}$ mice treated with vehicle or ginkgolide A. Each group consists of three age-matched male mice.

Data are presented as means ± SEM; n represents the numbers of tested mice in (B)–(H); n represents the numbers of recorded neurons in (J) and (L). Student's t test analysis was used in (B) and (D). One-way ANOVA analysis with Tukey's test was used in (C), (E)–(H), (J), and (L).

See also Figure S6.

## SUPPLEMENTAL INFORMATION

Supplemental Information can be found online at https://doi.org/10.1016/j.celrep.2020.03.085.

## ACKNOWLEDGMENTS

We appreciate the open access to SFARI Base (https://base.sfari.org), Allen Institute (https://alleninstitute.org), and BrainSpan atlas (http://www.brainspan.org). We are thankful for helpful suggestions from Professors Xiu Xu, Lan Bao, and Birong Liu. We acknowledge Prof. Jiada Li for proposals in the mouse behavioral tests. We thank Dr. Zhichao Wang for ideas in luciferase assay. We thank Prof. Zhengang Yang for providing the Gad1-GFP knockin mouse. This work was supported in part by the "Strategic Priority Research Program" of the Chinese Academy of Sciences (grants XDA16020501 and XDA16020404); the National Key Basic Research and Development Program of China (grants 2018YFA0800100, 2018YFA0108000, 2018YFA0107200, 2017YFA0102700, 2015CB964500, and 2014CB964804); and the National Natural Science Foundation of China (grants 31661143042, 91519314, 31630043, 31571513, 31430058, and 31900454) to N.J.; and by the National Natural Science Foundation of China (grant 31671508) to K.T.

## AUTHOR CONTRIBUTIONS

The authors contributed this study at different levels as follows: Study Conception and Design, K.Z., K.T., and N.J; Generation of Mutant Human Embryonic Stem Cell Lines, K.Z; Neuron Differentiation, K.Z. and Y.C.; Electrophysiology, S.H., W.G., L.C., X.W., and S.H; RNA-Seq and ChIP-Seq Sample Preparations, Y.C., K.Z., and X.Y; Generation of Mutant Mouse Strain, J.L., K.Z., and J.L; Immunostaining, T.S., J.Z., F.Y., and K.Z; Bioinformatic Analyses, J.C., R.W., K.Z., Y.Z., C.-C.H., and G.P; Mouse Behavioral Test, K.Z., F.Y., T.S., Y.Q., and J.Y; Manuscript Writing, K.Z., Y.C., J.C., J.Z., G.P., S.H., K.T., and N.J; all authors participated in the discussion of results and manuscript preparation.

## DECLARATION OF INTERESTS

The authors declare no competing interests.

Received: August 12, 2019
Revised: December 13, 2019
Accepted: March 24, 2020
Published: April 21, 2020

## REFERENCES

Abrahams, B.S., Arking, D.E., Campbell, D.B., Mefford, H.C., Morrow, E.M., Weiss, L.A., Menashe, I., Wadkins, T., Banerjee-Basu, S., and Packer, A. (2013). SFARI Gene 2.0: a community-driven knowledgebase for the autism spectrum disorders (ASDs). Mol. Autism *4*, 36.

Adhya, D., Swarup, V., Nagy, R., Shum, C., Nowosiad, P., Jozwik, K., Lee, I., Skuse, D., Flinter, F.A., McAlonan, G., et al. (2019). Atypical neurogenesis and excitatory-inhibitory progenitor generation in induced pluripotent stem cell (iPSC) from autistic individuals. bioRxiv. https://doi.org/10.1101/349415.

Al-Ayadhi, L.Y. (2012). Relationship between Sonic hedgehog protein, brain-derived neurotrophic factor and oxidative stress in autism spectrum disorders. Neurochem. Res. *37*, 394–400.

Alfano, C., Viola, L., Heng, J.I.-T., Pirozzi, M., Clarkson, M., Flore, G., De Maio, A., Schedl, A., Guillemot, F., and Studer, M. (2011). COUP-TFI promotes radial migration and proper morphology of callosal projection neurons by repressing Rnd2 expression. Development *138*, 4685–4697.

Armentano, M., Chou, S.J., Tomassy, G.S., Leingärtner, A., O'Leary, D.D., and Studer, M. (2007). COUP-TFI regulates the balance of cortical patterning between frontal/motor and sensory areas. Nat. Neurosci. *10*, 1277–1286.

Banerjee, A., Luong, J.A., Ho, A., Saib, A.O., and Ploski, J.E. (2016). Overexpression of Homer1a in the basal and lateral amygdala impairs fear conditioning and induces an autism-like social impairment. Mol. Autism *7*, 16.

Betancur, C. (2011). Etiological heterogeneity in autism spectrum disorders: more than 100 genetic and genomic disorders and still counting. Brain Res. *1380*, 42–77.

Bevins, R.A., and Besheer, J. (2006). Object recognition in rats and mice: a one-trial non-matching-to-sample learning task to study 'recognition memory'. Nat. Protoc. *1*, 1306–1311.

Bosch, D.G., Boonstra, F.N., Gonzaga-Jauregui, C., Xu, M., de Ligt, J., Jhangiani, S., Wiszniewski, W., Muzny, D.M., Yntema, H.G., Pfundt, R., et al.; Baylor-Hopkins Center for Mendelian Genomics (2014). NR2F1 mutations cause optic atrophy with intellectual disability. Am. J. Hum. Genet. *94*, 303–309.

Brakeman, P.R., Lanahan, A.A., O'Brien, R., Roche, K., Barnes, C.A., Huganir, R.L., and Worley, P.F. (1997). Homer: a protein that selectively binds metabotropic glutamate receptors. Nature *386*, 284–288.

Bruto, V., Beauchamp, C., Zacharko, R.M., and Anisman, H. (1984). Amphetamine-induced perseverative behavior in a radial arm maze following DSP4 or 6-OHDA pretreatment. Psychopharmacology (Berl.) *83*, 62–69.

Bulfone, A., Martinez, S., Marigo, V., Campanella, M., Basile, A., Quaderi, N., Gattuso, C., Rubenstein, J.L., and Ballabio, A. (1999). Expression pattern of the Tbr2 (Eomesodermin) gene during mouse and chick brain development. Mech. Dev. *84*, 133–138.

Buxbaum, J.D., Silverman, J.M., Smith, C.J., Greenberg, D.A., Kilifarski, M., Reichert, J., Cook, E.H., Jr., Fang, Y., Song, C.Y., and Vitale, R. (2002). Association between a GABRB3 polymorphism and autism. Mol. Psychiatry *7*, 311–316.

Campbell, K. (2003). Dorsal-ventral patterning in the mammalian telencephalon. Curr. Opin. Neurobiol. *13*, 50–56.

Casanova, M.F., Buxhoeveden, D., and Gomez, J. (2003). Disruption in the inhibitory architecture of the cell minicolumn: implications for autism. Neuroscientist *9*, 496–507.

Chakrabarti, L., Best, T.K., Cramer, N.P., Carney, R.S., Isaac, J.T., Galdzicki, Z., and Haydar, T.F. (2010). Olig1 and Olig2 triplication causes developmental brain defects in Down syndrome. Nat. Neurosci. *13*, 927–934.

Chang, S.C., Pauls, D.L., Lange, C., Sasanfar, R., and Santangelo, S.L. (2011). Common genetic variation in the GAD1 gene and the entire family of DLX homeobox genes and autism spectrum disorders. Am. J. Med. Genet. B. Neuropsychiatr. Genet. *156*, 233–239.

Chen, J.K., Taipale, J., Cooper, M.K., and Beachy, P.A. (2002). Inhibition of Hedgehog signaling by direct binding of cyclopamine to Smoothened. Genes Dev. *16*, 2743–2748.

Chen, C.-A., Bosch, D.G.M., Cho, M.T., Rosenfeld, J.A., Shinawi, M., Lewis, R.A., Mann, J., Jayakar, P., Payne, K., Walsh, L., et al. (2016). The expanding clinical phenotype of Bosch-Boonstra-Schaaf optic atrophy syndrome: 20 new cases and possible genotype-phenotype correlations. Genet. Med. *18*, 1143–1150.

Chen, R., Davis, L.K., Guter, S., Wei, Q., Jacob, S., Potter, M.H., Cox, N.J., Cook, E.H., Sutcliffe, J.S., and Li, B. (2017). Leveraging blood serotonin as an endophenotype to identify de novo and rare variants involved in autism. Mol. Autism *8*, 14.

Choii, G., and Ko, J. (2015). Gephyrin: a central GABAergic synapse organizer. Exp. Mol. Med. *47*, e158.

Collignon, O., Charbonneau, G., Peters, F., Nassim, M., Lassonde, M., Lepore, F., Mottron, L., and Bertone, A. (2013). Reduced multisensory facilitation in persons with autism. Cortex *49*, 1704–1710.

Conrad, C.D., Lupien, S.J., Thanasoulis, L.C., and McEwen, B.S. (1997). The effects of type I and type II corticosteroid receptor agonists on exploratory behavior and spatial memory in the Y-maze. Brain Res. *759*, 76–83.

Cooney, A.J., Tsai, S.Y., O'Malley, B.W., and Tsai, M.J. (1992). Chicken ovalbumin upstream promoter transcription factor (COUP-TF) dimers bind to different GGTCA response elements, allowing COUP-TF to repress hormonal induction of the vitamin D3, thyroid hormone, and retinoic acid receptors. Mol. Cell. Biol. *12*, 4153–4163.

Cossette, P., Liu, L., Brisebois, K., Dong, H., Lortie, A., Vanasse, M., Saint-Hilaire, J.M., Carmant, L., Verner, A., Lu, W.Y., et al. (2002). Mutation of GABRA1 in an autosomal dominant form of juvenile myoclonic epilepsy. Nat. Genet. *31*, 184–189.

Courchesne, E., Mouton, P.R., Calhoun, M.E., Semendeferi, K., Ahrens-Barbeau, C., Hallet, M.J., Barnes, C.C., and Pierce, K. (2011). Neuron number and size in prefrontal cortex of children with autism. JAMA *306*, 2001–2010.

Davis, L.K., Meyer, K.J., Rudd, D.S., Librant, A.L., Epping, E.A., Sheffield, V.C., and Wassink, T.H. (2008). Pax6 3′ deletion results in aniridia, autism and mental retardation. Hum. Genet. *123*, 371–378.

De Rubeis, S., He, X., Goldberg, A.P., Poultney, C.S., Samocha, K., Cicek, A.E., Kou, Y., Liu, L., Fromer, M., Walker, S., et al.; DDD Study; Homozygosity Mapping Collaborative for Autism; UK10K Consortium (2014). Synaptic, transcriptional and chromatin genes disrupted in autism. Nature *515*, 209–215.

DeRosa, B.A., El Hokayem, J., Artimovich, E., Garcia-Serje, C., Phillips, A.W., Van Booven, D., Nestor, J.E., Wang, L., Cuccaro, M.L., Vance, J.M., et al. (2018). Convergent pathways in idiopathic autism revealed by time course transcriptomic analysis of patient-derived neurons. Sci. Rep. *8*, 8423.

Eiraku, M., Watanabe, K., Matsuo-Takasaki, M., Kawada, M., Yonemura, S., Matsumura, M., Wataya, T., Nishiyama, A., Muguruma, K., and Sasai, Y. (2008). Self-organized formation of polarized cortical tissues from ESCs and its active manipulation by extrinsic signals. Cell Stem Cell *3*, 519–532.

Elkabetz, Y., Panagiotakos, G., Al Shamy, G., Socci, N.D., Tabar, V., and Studer, L. (2008). Human ES cell-derived neural rosettes reveal a functionally distinct early neural stem cell stage. Genes Dev. *22*, 152–165.

Ellis, P., Fagan, B.M., Magness, S.T., Hutton, S., Taranova, O., Hayashi, S., McMahon, A., Rao, M., and Pevny, L. (2004). SOX2, a persistent marker for multipotential neural stem cells derived from embryonic stem cells, the embryo or the adult. Dev. Neurosci. *26*, 148–165.

Etherton, M., Földy, C., Sharma, M., Tabuchi, K., Liu, X., Shamloo, M., Malenka, R.C., and Südhof, T.C. (2011). Autism-linked neuroligin-3 R451C mutation differentially alters hippocampal and cortical synaptic function. Proc. Natl. Acad. Sci. USA *108*, 13764–13769.

Farkas, L.M., Dünker, N., Roussa, E., Unsicker, K., and Krieglstein, K. (2003). Transforming growth factor-β(s) are essential for the development of midbrain dopaminergic neurons in vitro and in vivo. J. Neurosci. *23*, 5178–5186.

Fatemi, S.H., and Halt, A.R. (2001). Altered levels of Bcl2 and p53 proteins in parietal cortex reflect deranged apoptotic regulation in autism. Synapse *42*, 281–284.

Fatemi, S.H., Folsom, T.D., Reutiman, T.J., and Thuras, P.D. (2009). Expression of $GABA_B$ receptors is altered in brains of subjects with autism. Cerebellum *8*, 64–69.

Feng, S., Xing, C., Shen, T., Qiao, Y., Wang, R., Chen, J., Liao, J., Lu, Z., Yang, X., Abd-Allah, S.M., et al. (2017). Abnormal paraventricular nucleus of hypothalamus and growth retardation associated with loss of nuclear receptor gene COUP-TFII. Sci. Rep. *7*, 5282.

Fernandez, F., Morishita, W., Zuniga, E., Nguyen, J., Blank, M., Malenka, R.C., and Garner, C.C. (2007). Pharmacotherapy for cognitive impairment in a mouse model of Down syndrome. Nat. Neurosci. *10*, 411–413.

Fode, C., Ma, Q., Casarosa, S., Ang, S.-L., Anderson, D.J., and Guillemot, F. (2000). A role for neural determination genes in specifying the dorsoventral identity of telencephalic neurons. Genes Dev. *14*, 67–80.

Fremeau, R.T., Jr., Troyer, M.D., Pahner, I., Nygaard, G.O., Tran, C.H., Reimer, R.J., Bellocchio, E.E., Fortin, D., Storm-Mathisen, J., and Edwards, R.H. (2001). The expression of vesicular glutamate transporters defines two classes of excitatory synapse. Neuron *31*, 247–260.

Galaburda, A.M., Schmitt, J.E., Atlas, S.W., Eliez, S., Bellugi, U., and Reiss, A.L. (2001). Dorsal forebrain anomaly in Williams syndrome. Arch. Neurol. *58*, 1865–1869.

Garcia, A.D.R., Doan, N.B., Imura, T., Bush, T.G., and Sofroniew, M.V. (2004). GFAP-expressing progenitors are the principal source of constitutive neurogenesis in adult mouse forebrain. Nat. Neurosci. *7*, 1233–1241.

Geschwind, D.H. (2009). Advances in autism. Annu. Rev. Med. *60*, 367–380.

Gogolla, N., Leblanc, J.J., Quast, K.B., Südhof, T.C., Fagiolini, M., and Hensch, T.K. (2009). Common circuit defect of excitatory-inhibitory balance in mouse models of autism. J. Neurodev. Disord. *1*, 172–181.

Han, S., Tai, C., Westenbroek, R.E., Yu, F.H., Cheah, C.S., Potter, G.B., Rubenstein, J.L., Scheuer, T., de la Iglesia, H.O., and Catterall, W.A. (2012). Autistic-like behaviour in $Scn1a^{+/-}$ mice and rescue by enhanced GABA-mediated neurotransmission. Nature *489*, 385–390.

Han, S., Tai, C., Jones, C.J., Scheuer, T., and Catterall, W.A. (2014). Enhancement of inhibitory neurotransmission by GABAA receptors having α2,3-subunits ameliorates behavioral deficits in a mouse model of autism. Neuron *81*, 1282–1289.

Hevner, R.F., Hodge, R.D., Daza, R.A., and Englund, C. (2006). Transcription factors in glutamatergic neurogenesis: conserved programs in neocortex, cerebellum, and adult hippocampus. Neurosci. Res. *55*, 223–233.

Hong, F., Breitling, R., McEntee, C.W., Wittner, B.S., Nemhauser, J.L., and Chory, J. (2006). RankProd: a bioconductor package for detecting differentially expressed genes in meta-analysis. Bioinformatics *22*, 2825–2827.

Hu, J.S., Vogt, D., Lindtner, S., Sandberg, M., Silberberg, S.N., and Rubenstein, J.L.R. (2017). *Coup-TF1* and *Coup-TF2* control subtype and laminar identity of MGE-derived neocortical interneurons. Development *144*, 2837–2851.

Huang, T.-N., and Hsueh, Y.-P. (2014). Novel object recognition for studying memory in mice. Bio- Protoc. *4*, e1249.

Huang, S.H., Duke, R.K., Chebib, M., Sasaki, K., Wada, K., and Johnston, G.A. (2004). Ginkgolides, diterpene trilactones of *Ginkgo biloba*, as antagonists at recombinant α1β2γ2L GABAA receptors. Eur. J. Pharmacol. *494*, 131–138.

Johnson, M.A., Weick, J.P., Pearce, R.A., and Zhang, S.-C. (2007). Functional neural development from human embryonic stem cells: accelerated synaptic activity via astrocyte coculture. J. Neurosci. *27*, 3069–3077.

Johnston, J.J., Sapp, J.C., Turner, J.T., Amor, D., Aftimos, S., Aleck, K.A., Bocian, M., Bodurtha, J.N., Cox, G.F., Curry, C.J., et al. (2010). Molecular analysis expands the spectrum of phenotypes associated with GLI3 mutations. Hum. Mutat. *31*, 1142–1154.

Kaneko, Y., Sakakibara, S., Imai, T., Suzuki, A., Nakamura, Y., Sawamoto, K., Ogawa, Y., Toyama, Y., Miyata, T., and Okano, H. (2000). Musashi1: an evolutionally conserved marker for CNS progenitor cells including neural stem cells. Dev. Neurosci. *22*, 139–153.

Kang, H.J., Kawasawa, Y.I., Cheng, F., Zhu, Y., Xu, X., Li, M., Sousa, A.M., Pletikos, M., Meyer, K.A., Sedmak, G., et al. (2011). Spatio-temporal transcriptome of the human brain. Nature *478*, 483–489.

Katoh, Y., and Katoh, M. (2009). Hedgehog target genes: mechanisms of carcinogenesis induced by aberrant hedgehog signaling activation. Curr. Mol. Med. *9*, 873–886.

Kemper, T.L., and Bauman, M. (1998). Neuropathology of infantile autism. J. Neuropathol. Exp. Neurol. *57*, 645–652.

Kessaris, N., Magno, L., Rubin, A.N., and Oliveira, M.G. (2014). Genetic programs controlling cortical interneuron fate. Curr. Opin. Neurobiol. *26*, 79–87.

Kortüm, F., Das, S., Flindt, M., Morris-Rosendahl, D.J., Stefanova, I., Goldstein, A., Horn, D., Klopocki, E., Kluger, G., Martin, P., et al. (2011). The core *FOXG1* syndrome phenotype consists of postnatal microcephaly, severe mental retardation, absent language, dyskinesia, and corpus callosum hypogenesis. J. Med. Genet. *48*, 396–406.

Kuribara, H., Weintraub, S.T., Yoshihama, T., and Maruyama, Y. (2003). An anxiolytic-like effect of Ginkgo biloba extract and its constituent, ginkgolide-A, in mice. J. Nat. Prod. *66*, 1333–1337.

Langmead, B., and Salzberg, S.L. (2012). Fast gapped-read alignment with Bowtie 2. Nat. Methods *9*, 357–359.

Lawrence, Y.A., Kemper, T.L., Bauman, M.L., and Blatt, G.J. (2010). Parvalbumin-, calbindin-, and calretinin-immunoreactive hippocampal interneuron density in autism. Acta Neurol. Scand. *121*, 99–108.

Lee, J., Platt, K.A., Censullo, P., and Ruiz i Altaba, A. (1997). Gli1 is a target of Sonic hedgehog that induces ventral neural tube development. Development *124*, 2537–2552.

Leger, M., Quiedeville, A., Bouet, V., Haelewyn, B., Boulouard, M., Schumann-Bard, P., and Freret, T. (2013). Object recognition test in mice. Nat. Protoc. *8*, 2531–2537.

Leone, D.P., Srinivasan, K., Chen, B., Alcamo, E., and McConnell, S.K. (2008). The determination of projection neuron identity in the developing cerebral cortex. Curr. Opin. Neurobiol. *18*, 28–35.

Li, X.J., Zhang, X., Johnson, M.A., Wang, Z.B., Lavaute, T., and Zhang, S.C. (2009). Coordination of sonic hedgehog and Wnt signaling determines ventral and dorsal telencephalic neuron types from human embryonic stem cells. Development *136*, 4055–4063.

Li, Y., Wang, R., Qiao, N., Peng, G., Zhang, K., Tang, K., Han, J.J., and Jing, N. (2017a). Transcriptome analysis reveals determinant stages controlling human embryonic stem cell commitment to neuronal cells. J. Biol. Chem. *292*, 19590–19604.

Li, Y., Wu, Y., Yao, X., Hao, F., Yu, C., Bao, Y., Wu, Y., Song, Z., Sun, Y., Zheng, L., et al. (2017b). Ginkgolide A ameliorates LPS-induced inflammatory responses *in vitro* and *in vivo*. Int. J. Mol. Sci. *18*, 794.

Lim, E.T., Uddin, M., De Rubeis, S., Chan, Y., Kamumbu, A.S., Zhang, X., D'Gama, A.M., Kim, S.N., Hill, R.S., Goldberg, A.P., et al.; Autism Sequencing Consortium (2017). Rates, distribution and implications of postzygotic mosaic mutations in autism spectrum disorder. Nat. Neurosci. *20*, 1217–1224.

Liu, X., Novosedlik, N., Wang, A., Hudson, M.L., Cohen, I.L., Chudley, A.E., Forster-Gibson, C.J., Lewis, S.M., and Holden, J.J. (2009). The DLX1and DLX2 genes and susceptibility to autism spectrum disorders. Eur. J. Hum. Genet. *17*, 228–235.

Livide, G., Patriarchi, T., Amenduni, M., Amabile, S., Yasui, D., Calcagno, E., Lo Rizzo, C., De Falco, G., Ulivieri, C., Ariani, F., et al. (2015). GluD1 is a common altered player in neuronal differentiation from both MECP2-mutated and CDKL5-mutated iPS cells. Eur. J. Hum. Genet. *23*, 195–201.

Love, M.I., Huber, W., and Anders, S. (2014). Moderated estimation of fold change and dispersion for RNA-seq data with DESeq2. Genome Biol. *15*, 550.

Lu, J.T., Li, C.Y., Zhao, J.P., Poo, M.M., and Zhang, X.H. (2007). Spike-timing-dependent plasticity of neocortical excitatory synapses on inhibitory interneurons depends on target cell type. J. Neurosci. *27*, 9711–9720.

Marco, E.J., Khatibi, K., Hill, S.S., Siegel, B., Arroyo, M.S., Dowling, A.F., Neuhaus, J.M., Sherr, E.H., Hinkley, L.N., and Nagarajan, S.S. (2012). Children with autism show reduced somatosensory response: an MEG study. Autism Res. *5*, 340–351.

Mariani, J., Simonini, M.V., Palejev, D., Tomasini, L., Coppola, G., Szekely, A.M., Horvath, T.L., and Vaccarino, F.M. (2012). Modeling human cortical development in vitro using induced pluripotent stem cells. Proc. Natl. Acad. Sci. USA *109*, 12770–12775.

Mariani, J., Coppola, G., Zhang, P., Abyzov, A., Provini, L., Tomasini, L., Amenduni, M., Szekely, A., Palejev, D., Wilson, M., et al. (2015). FOXG1-DEPENDENT DYSREGULATION of GABA/glutamate neuron differentiation in autism spectrum disorders. Cell *162*, 375–390.

Marín, O., and Rubenstein, J.L. (2001). A long, remarkable journey: tangential migration in the telencephalon. Nat. Rev. Neurosci. *2*, 780–790.

Markram, K., Rinaldi, T., La Mendola, D., Sandi, C., and Markram, H. (2008). Abnormal fear conditioning and amygdala processing in an animal model of autism. Neuropsychopharmacology *33*, 901–912.

Martynoga, B., Morrison, H., Price, D.J., and Mason, J.O. (2005). Foxg1 is required for specification of ventral telencephalon and region-specific regulation of dorsal telencephalic precursor proliferation and apoptosis. Dev. Biol. *283*, 113–127.

McLean, C.Y., Bristor, D., Hiller, M., Clarke, S.L., Schaar, B.L., Lowe, C.B., Wenger, A.M., and Bejerano, G. (2010). GREAT improves functional interpretation of cis-regulatory regions. Nat. Biotechnol. *28*, 495–501.

Molyneaux, B.J., Arlotta, P., Menezes, J.R., and Macklis, J.D. (2007). Neuronal subtype specification in the cerebral cortex. Nat. Rev. Neurosci. *8*, 427–437.

Mootha, V.K., Lindgren, C.M., Eriksson, K.F., Subramanian, A., Sihag, S., Lehar, J., Puigserver, P., Carlsson, E., Ridderstråle, M., Laurila, E., et al. (2003). PGC-1α-responsive genes involved in oxidative phosphorylation are coordinately downregulated in human diabetes. Nat. Genet. *34*, 267–273.

Morozov, Y.M., Torii, M., and Rakic, P. (2009). Origin, early commitment, migratory routes, and destination of cannabinoid type 1 receptor-containing interneurons. Cereb. Cortex *19* (*Suppl 1*), i78–i89.

Motoyama, J., and Aoto, K. (2006). Important role of Shh controlling Gli3 functions during the dorsal-ventral patterning of the telencephalon. In Hedgehog-Gli Signaling in Human Disease, A.R.i. Altaba, ed. (Springer), pp. 177–186.

Mukhopadhyay, S., Wen, X., Ratti, N., Loktev, A., Rangell, L., Scales, S.J., and Jackson, P.K. (2013). The ciliary G-protein-coupled receptor Gpr161 negatively regulates the Sonic hedgehog pathway via cAMP signaling. Cell *152*, 210–223.

Naka, H., Nakamura, S., Shimazaki, T., and Okano, H. (2008). Requirement for COUP-TFI and II in the temporal specification of neural stem cells in CNS development. Nat. Neurosci. *11*, 1014–1023.

Nieto, M., Monuki, E.S., Tang, H., Imitola, J., Haubst, N., Khoury, S.J., Cunningham, J., Gotz, M., and Walsh, C.A. (2004). Expression of Cux-1 and Cux-2 in the subventricular zone and upper layers II-IV of the cerebral cortex. J. Comp. Neurol. *479*, 168–180.

Noor, A., Whibley, A., Marshall, C.R., Gianakopoulos, P.J., Piton, A., Carson, A.R., Orlic-Milacic, M., Lionel, A.C., Sato, D., Pinto, D., et al. (2010). Disruption at the PTCHD1 locus on Xp22.11 in autism spectrum disorder and intellectual disability. Sci. Transl. Med. *2*, 49ra68.

O'Leary, D.D., and Nakagawa, Y. (2002). Patterning centers, regulatory genes and extrinsic mechanisms controlling arealization of the neocortex. Curr. Opin. Neurobiol. *12*, 14–25.

O'Roak, B.J., Vives, L., Girirajan, S., Karakoc, E., Krumm, N., Coe, B.P., Levy, R., Ko, A., Lee, C., Smith, J.D., et al. (2012). Sporadic autism exomes reveal a highly interconnected protein network of de novo mutations. Nature *485*, 246–250.

Pankratz, M.T., Li, X.J., Lavaute, T.M., Lyons, E.A., Chen, X., and Zhang, S.C. (2007). Directed neural differentiation of human embryonic stem cells via an obligated primitive anterior stage. Stem Cells *25*, 1511–1520.

Parikshak, N.N., Luo, R., Zhang, A., Won, H., Lowe, J.K., Chandran, V., Horvath, S., and Geschwind, D.H. (2013). Integrative functional genomic analyses implicate specific molecular pathways and circuits in autism. Cell *155*, 1008–1021.

Peng, G., Suo, S., Chen, J., Chen, W., Liu, C., Yu, F., Wang, R., Chen, S., Sun, N., Cui, G., et al. (2016). Spatial transcriptome for the molecular annotation of lineage fates and cell identity in mid-gastrula mouse embryo. Dev. Cell *36*, 681–697.

Persico, A.M., D'Agruma, L., Maiorano, N., Totaro, A., Militerni, R., Bravaccio, C., Wassink, T.H., Schneider, C., Melmed, R., Trillo, S., et al.; Collaborative

Linkage Study of Autism (2001). Reelin gene alleles and haplotypes as a factor predisposing to autistic disorder. Mol. Psychiatry *6*, 150–159.

Qiao, Y., Wang, R., Yang, X., Tang, K., and Jing, N. (2015). Dual roles of histone H3 lysine 9 acetylation in human embryonic stem cell pluripotency and neural differentiation. J. Biol. Chem. *290*, 2508–2520.

Rallu, M., Machold, R., Gaiano, N., Corbin, J.G., McMahon, A.P., and Fishell, G. (2002). Dorsoventral patterning is established in the telencephalon of mutants lacking both Gli3 and Hedgehog signaling. Development *129*, 4963–4974.

Ran, F.A., Hsu, P.D., Wright, J., Agarwala, V., Scott, D.A., and Zhang, F. (2013). Genome engineering using the CRISPR-Cas9 system. Nat. Protoc. *8*, 2281–2308.

Rogers, M.B., Hosler, B.A., and Gudas, L.J. (1991). Specific expression of a retinoic acid-regulated, zinc-finger gene, Rex-1, in preimplantation embryos, trophoblast and spermatocytes. Development *113*, 815–824.

Rubenstein, J.L. (2010). Three hypotheses for developmental defects that may underlie some forms of autism spectrum disorder. Curr. Opin. Neurol. *23*, 118–123.

Rubenstein, J.L., and Merzenich, M.M. (2003). Model of autism: increased ratio of excitation/inhibition in key neural systems. Genes Brain Behav. *2*, 255–267.

Sahraeian, S.M.E., Mohiyuddin, M., Sebra, R., Tilgner, H., Afshar, P.T., Au, K.F., Bani Asadi, N., Gerstein, M.B., Wong, W.H., Snyder, M.P., et al. (2017). Gaining comprehensive biological insight into the transcriptome by performing a broad-spectrum RNA-seq analysis. Nat. Commun. *8*, 59.

Sanders, S.J., Murtha, M.T., Gupta, A.R., Murdoch, J.D., Raubeson, M.J., Willsey, A.J., Ercan-Sencicek, A.G., DiLullo, N.M., Parikshak, N.N., Stein, J.L., et al. (2012). *De novo* mutations revealed by whole-exome sequencing are strongly associated with autism. Nature *485*, 237–241.

Sandhu, K.V., Lang, D., Müller, B., Nullmeier, S., Yanagawa, Y., Schwegler, H., and Stork, O. (2014). Glutamic acid decarboxylase 67 haplodeficiency impairs social behavior in mice. Genes Brain Behav. *13*, 439–450.

Sheng, T., Li, C., Zhang, X., Chi, S., He, N., Chen, K., McCormick, F., Gatalica, Z., and Xie, J. (2004). Activation of the hedgehog pathway in advanced prostate cancer. Mol. Cancer *3*, 29.

Shi, W., Wang, H., Pan, G., Geng, Y., Guo, Y., and Pei, D. (2006). Regulation of the pluripotency marker Rex-1 by Nanog and Sox2. J. Biol. Chem. *281*, 23319–23325.

Siracusano, M., Riccioni, A., Baratta, A., Baldi, M., Curatolo, P., and Mazzone, L. (2019). Autistic symptoms in Greig cephalopolysyndactyly syndrome: a family case report. J. Med. Case Reports *13*, 100.

Smith, S.E., Zhou, Y.D., Zhang, G., Jin, Z., Stoppel, D.C., and Anderson, M.P. (2011). Increased gene dosage of Ube3a results in autism traits and decreased glutamate synaptic transmission in mice. Sci. Transl. Med. *3*, 103ra97.

Smith, C., Gore, A., Yan, W., Abalde-Atristain, L., Li, Z., He, C., Wang, Y., Brodsky, R.A., Zhang, K., Cheng, L., and Ye, Z. (2014). Whole-genome sequencing analysis reveals high specificity of CRISPR/Cas9 and TALEN-based genome editing in human iPSCs. Cell Stem Cell *15*, 12–13.

Srikanth, P., Han, K., Callahan, D.G., Makovkina, E., Muratore, C.R., Lalli, M.A., Zhou, H., Boyd, J.D., Kosik, K.S., Selkoe, D.J., and Young-Pearse, T.L. (2015). Genomic DISC1 disruption in hiPSCs alters Wnt signaling and neural cell fate. Cell Rep. *12*, 1414–1429.

Subramanian, A., Tamayo, P., Mootha, V.K., Mukherjee, S., Ebert, B.L., Gillette, M.A., Paulovich, A., Pomeroy, S.L., Golub, T.R., Lander, E.S., and Mesirov, J.P. (2005). Gene set enrichment analysis: a knowledge-based approach for interpreting genome-wide expression profiles. Proc. Natl. Acad. Sci. USA *102*, 15545–15550.

Südhof, T.C. (2008). Neuroligins and neurexins link synaptic function to cognitive disease. Nature *455*, 903–911.

Tabuchi, K., Blundell, J., Etherton, M.R., Hammer, R.E., Liu, X., Powell, C.M., and Südhof, T.C. (2007). A neuroligin-3 mutation implicated in autism increases inhibitory synaptic transmission in mice. Science *318*, 71–76.

Takahashi, K., Tanabe, K., Ohnuki, M., Narita, M., Ichisaka, T., Tomoda, K., and Yamanaka, S. (2007). Induction of pluripotent stem cells from adult human fibroblasts by defined factors. Cell *131*, 861–872.

Tamamaki, N., Yanagawa, Y., Tomioka, R., Miyazaki, J., Obata, K., and Kaneko, T. (2003). Green fluorescent protein expression and colocalization with calretinin, parvalbumin, and somatostatin in the GAD67-GFP knock-in mouse. J. Comp. Neurol. *467*, 60–79.

Theil, T., Alvarez-Bolado, G., Walter, A., and Rüther, U. (1999). Gli3 is required for Emx gene expression during dorsal telencephalon development. Development *126*, 3561–3571.

Thomson, J.A., Itskovitz-Eldor, J., Shapiro, S.S., Waknitz, M.A., Swiergiel, J.J., Marshall, V.S., and Jones, J.M. (1998). Embryonic stem cell lines derived from human blastocysts. Science *282*, 1145–1147.

Veres, A., Gosis, B.S., Ding, Q., Collins, R., Ragavendran, A., Brand, H., Erdin, S., Cowan, C.A., Talkowski, M.E., and Musunuru, K. (2014). Low incidence of off-target mutations in individual CRISPR-Cas9 and TALEN targeted human stem cell clones detected by whole-genome sequencing. Cell Stem Cell *15*, 27–30.

Willsey, A.J., Sanders, S.J., Li, M., Dong, S., Tebbenkamp, A.T., Muhle, R.A., Reilly, S.K., Lin, L., Fertuzinhos, S., Miller, J.A., et al. (2013). Coexpression networks implicate human midfetal deep cortical projection neurons in the pathogenesis of autism. Cell *155*, 997–1007.

Wilson, S.W., and Rubenstein, J.L. (2000). Induction and dorsoventral patterning of the telencephalon. Neuron *28*, 641–651.

Wonders, C.P., and Anderson, S.A. (2006). The origin and specification of cortical interneurons. Nat. Rev. Neurosci. *7*, 687–696.

Wu, Y., Liang, D., Wang, Y., Bai, M., Tang, W., Bao, S., Yan, Z., Li, D., and Li, J. (2013). Correction of a genetic disease in mouse via use of CRISPR-Cas9. Cell Stem Cell *13*, 659–662.

Yang, X., Hu, B., Hou, Y., Qiao, Y., Wang, R., Chen, Y., Qian, Y., Feng, S., Chen, J., Liu, C., et al. (2018). Silencing of developmental genes by H3K27me3 and DNA methylation reflects the discrepant plasticity of embryonic and extraembryonic lineages. Cell Res. *28*, 593–596.

Yizhar, O., Fenno, L.E., Prigge, M., Schneider, F., Davidson, T.J., O'Shea, D.J., Sohal, V.S., Goshen, I., Finkelstein, J., Paz, J.T., et al. (2011). Neocortical excitation/inhibition balance in information processing and social dysfunction. Nature *477*, 171–178.

Yu, G., Wang, L.-G., Han, Y., and He, Q.-Y. (2012). clusterProfiler: an R package for comparing biological themes among gene clusters. OMICS *16*, 284–287.

Zhang, S.-C., Wernig, M., Duncan, I.D., Brüstle, O., and Thomson, J.A. (2001). In vitro differentiation of transplantable neural precursors from human embryonic stem cells. Nat. Biotechnol. *19*, 1129–1133.

Zhang, Y., Liu, T., Meyer, C.A., Eeckhoute, J., Johnson, D.S., Bernstein, B.E., Nusbaum, C., Myers, R.M., Brown, M., Li, W., and Liu, X.S. (2008). Model-based analysis of ChIP-seq (MACS). Genome Biol. *9*, R137.

Zhang, X., Huang, C.T., Chen, J., Pankratz, M.T., Xi, J., Li, J., Yang, Y., Lavaute, T.M., Li, X.-J., Ayala, M., et al. (2010). Pax6 is a human neuroectoderm cell fate determinant. Cell Stem Cell *7*, 90–100.

Zhang, Y., Ho, T.N.T., Harvey, R.J., Lynch, J.W., and Keramidas, A. (2017). Structure-function analysis of the GlyR $\alpha$2 subunit autism mutation p. R323L reveals a gain-of-function. Front. Mol. Neurosci. *10*, 158.

Zhao, Q., Gao, C., and Cui, Z. (2015). Ginkgolide A reduces inflammatory response in high-glucose-stimulated human umbilical vein endothelial cells through STAT3-mediated pathway. Int. Immunopharmacol. *25*, 242–248.

Zhou, C., Qiu, Y., Pereira, F.A., Crair, M.C., Tsai, S.Y., and Tsai, M.J. (1999). The nuclear orphan receptor COUP-TFI is required for differentiation of subplate neurons and guidance of thalamocortical axons. Neuron *24*, 847–859.

Zhou, C., Tsai, S.Y., and Tsai, M.J. (2001). COUP-TFI: an intrinsic factor for early regionalization of the neocortex. Genes Dev. *15*, 2054–2059.

Zhu, Q., Song, L., Peng, G., Sun, N., Chen, J., Zhang, T., Sheng, N., Tang, W., Qian, C., Qiao, Y., et al. (2014). The transcription factor Pou3f1 promotes neural fate commitment via activation of neural lineage genes and inhibition of external signaling pathways. eLife *3*, e02224.

Zoghbi, H.Y., and Bear, M.F. (2012). Synaptic dysfunction in neurodevelopmental disorders associated with autism and intellectual disabilities. Cold Spring Harb. Perspect. Biol. *4*, a009886.

## STAR★METHODS

### KEY RESOURCES TABLE

| REAGENT or RESOURCE | SOURCE | IDENTIFIER |
|---|---|---|
| Antibodies | | |
| Mouse anti-Oct3/4 | Santa Cruz | Cat# sc-5279, RRID:AB_628051 |
| Goat anti-NANOG | R&D systems | Cat# AF1997, RRID:AB_355097 |
| Rabbit anti-SOX2 | Abcam | Cat# ab97959, RRID:AB_2341193 |
| Rabbit anti-PAX6 | EMD Millipore | Cat# AB2237, RRID:AB_1587367 |
| Rabbit anti-MUSASHI1 | Abcam | Cat# ab52865, RRID:AB_881168 |
| Goat anti-FABP7 | R&D systems | Cat# AF3166, RRID:AB_2100475 |
| Rabbit anti-TBR1 | Abcam | Cat# ab31940, RRID:AB_2200219 |
| Rabbit anti-DLX1/2 | A gift from Dr. Morozov Yuri | N/A |
| Mouse anti-NKX2.1 | EMD Millipore | Cat# MAB5460, RRID:AB_571072 |
| Rabbit anti-NKX2.1 | Abcam | Cat# ab76013, RRID:AB_1310784 |
| Goat anti-NGN1 | Santa Cruz | Cat# sc-19231, RRID:AB_2298242 |
| Rabbit anti-VGLUT1 | Synaptic Systems | Cat# 135 302, RRID:AB_887877 |
| Mouse anti-VGLUT1 | EMD Millipore | Cat# MAB5502, RRID:AB_262185 |
| Rabbit anti-VGAT | Synaptic Systems | Cat# 131 002, RRID:AB_887871 |
| Mouse anti-TUJ1 | Covance | Cat# MMS-435P, RRID:AB_2313773 |
| Rabbit anti-TUJ1 | Covance | Cat# MRB-435P-100, RRID:AB_663339 |
| Rabbit anti-GAD1/2 | EMD Millipore | Cat# AB1511, RRID:AB_90715 |
| Rabbit anti-GAD1/2 | Sigma-Aldrich | Cat# G5163, RRID:AB_477019 |
| Mouse anti-GAD1 | EMD Millipore | Cat# MAB5406, RRID:AB_2278725 |
| Mouse anti-GEPHYRIN | Synaptic Systems | Cat# 147 011, RRID:AB_887717 |
| Mouse anti-HOMER1 | Synaptic Systems | Cat# 160 011, RRID:AB_2120992 |
| Mouse anti-GluR2 | NeuroMab | Cat# 75-002, RRID:AB_2232661 |
| Rabbit anti-Cux1 | Santa Cruz | Cat# sc-13024, RRID:AB_2261231 |
| Rabbit anti-Ctip2 | Abcam | Cat# ab18465, RRID:AB_2064130 |
| Rabbit anti-PV | Abcam | Cat# ab11427, RRID:AB_298032 |
| Rabbit anti-GAPDH | Abcam | Cat# ab9485, RRID:AB_307275 |
| Mouse anti-NR2F1 | R&D systems | Cat# PP-H8132-00, RRID:AB_2155494 |
| Rabbit anti-Flag | Sigma-Aldrich | Cat# F7425, RRID:AB_439687 |
| Rabbit anti-SST | Peninsula Laboratories | Cat# T-4103.0050, RRID:AB_518614 |
| Bacterial and Virus Strains | | |
| *E. coli*. DH5a | TIANGEN Biotech | Cat# CB101 |
| Chemicals, Peptides, and Recombinant Proteins | | |
| DMEM, High glucose | GIBCO | Cat# 11965092 |
| DMEM/F-12, HEPES | GIBCO | Cat# 11330057 |
| Neurobasal Medium | GIBCO | Cat# 21103049 |
| KSOM Embryo Medium | EMD Millipore | Cat# MR-101-D |
| Knockout Serum Replacement (KSR) | GIBCO | Cat# 10828028 |
| Fetal Bovine Serum | GIBCO | Cat# 16000044 |
| N-2 Supplement (100X) | GIBCO | Cat# 17502048 |
| B-27 Supplement (50X), minus vitamin A | GIBCO | Cat# 12587010 |
| NEAA | GIBCO | Cat# 11140050 |
| GlutaMAX | GIBCO | Cat# 35050061 |
| β-Mercaptoethanol | Sigma-Aldrich | Cat# M3148 |

(*Continued on next page*)

*Continued*

| REAGENT or RESOURCE | SOURCE | IDENTIFIER |
|---|---|---|
| Penicillin/streptomycin | GIBCO | Cat# 15140122 |
| Trypsin (2.5%) | GIBCO | Cat# 15090046 |
| Basic FGF | Pufei Bio. | Cat# 1106-010 |
| BDNF | PeproTech | Cat# 450-02 |
| GDNF | PeproTech | Cat# 450-10 |
| NT-3 | PeproTech | Cat# 450-03 |
| Cyclopamine | Selleck | Cat# S1146 |
| Trizol | Pufei Bio | Cat# 3101-400 |
| Collagenase | GIBCO | Cat# 17104019 |
| Matrigel | Corning | Cat# 354230 |
| Accutase | GIBCO | Cat# A1110501 |
| Protein Ladder | Thermo Fisher | Cat# 26616 |
| Anti-FLAG Magnetic Beads | Sigma-Aldrich | Cat# M8823 |
| Ginkgolide A | Selleck | Cat# S2026 |
| Critical Commercial Assays | | |
| Lipofectamine Stem Transfection Reagent | Invitrogen | Cat# STEM00003 |
| SuperScript III First-strand cDNA synthesis kit | Invitrogen | Cat# 18080044 |
| Stormstar SYBR Green qPCR MasterMix | DBI Bioscience | Cat# DBI-2143 |
| NEBNext Ultra DNA Library Prep Kit for Illumina | NEB | Cat# E7370S |
| Dual-Glo TM luciferase assay system | Promega | Cat# E2920 |
| mMESSAGE mMACHINE T7 ULTRA kit | Invitrogen | Cat# AM1345 |
| MEGAshortscript T7 kit | Invitrogen | Cat# AM1354 |
| MEGAclear kit | Invitrogen | Cat# AM1908 |
| SuperSignal West Pico Substrate | Thermo Scientific | Cat# 34080 |
| Deposited Data | | |
| RNA- and ChIP-Seq data | This paper | GSE132965 |
| Experimental Models: Cell Lines | | |
| human fetal kidney fibroblast cell line 293T | Stem Cell Bank, Chines Academy of Sciences in Shanghai | Cat# SCSP-502 |
| CF-1 mouse embryonic fibroblast cells | Stem Cell Bank, Chines Academy of Sciences in Shanghai | Cat# SCSP-105 |
| H9 human embryonic stem cells | Stem Cell Bank, Chines Academy of Sciences in Shanghai | Cat# SCSP-302 |
| Experimental Models: Organisms/Strains | | |
| Mouse: C57BL/6 | Shanghai SLAC laboratory animal company | Cat# SKD111018 |
| Mouse: *Gad67-GFP* | Tamamaki et al., 2003 | N/A |
| Oligonucleotides | | |
| qPCR Primers | Table S4 | N/A |
| Donor Template for Gene Editing | Table S4 | N/A |
| Recombinant DNA | | |
| pcDNA3.1$^{+}$-WT(Mut) NR2F1-Flag | This paper | N/A |
| pGL3-GLI3 promoter | This paper | N/A |
| pGL3-GLI1 promoter | This paper | N/A |
| pGL3-SHH enhancer | This paper | N/A |
| pGL3-PTCH1 promoter | This paper | N/A |

(*Continued on next page*)

*Continued*

| REAGENT or RESOURCE | SOURCE | IDENTIFIER |
|---|---|---|
| Software and Algorithms | | |
| ImageJ | ImageJ | https://imagej.nih.gov/ij/download.html |
| Graphpad Prism 6 | GraphPad Software | https://www.graphpad.com/scientific-software/prism/ |
| pClampfit (version 10.6) | Molecular devices | https://www.moleculardevices.com/products/axon-patch-clamp-system/acquisition-and-analysis-software/pclamp-software-suite |
| HISAT2 (version 2.1.0) | Sahraeian et al., 2017 | http://daehwankimlab.github.io/hisat2/main/ |
| FeatureCounts (version 1.5.3) | Sahraeian et al., 2017 | http://subread.sourceforge.net |
| DESeq2 (version 1.16.1) | Love et al., 2014 | https://bioconductor.org/packages/release/bioc/html/DESeq2.html |
| clusterProfiler (version 3.4.4) | Yu et al., 2012 | https://bioconductor.org/packages/release/bioc/html/clusterProfiler.html |
| RankProd (version 3.2.0) | Hong et al., 2006 | http://bioconductor.org/packages/release/bioc/html/RankProd.html |
| Bowtie2 (version 2.3.1) | Langmead and Salzberg, 2012 | http://bowtie-bio.sourceforge.net/bowtie2/index.shtml |
| MACS2 (version 2.1.1) | Zhang et al., 2008 | https://github.com/taoliu/MACS/ |
| GREAT | McLean et al., 2010 | http://bejerano.stanford.edu/great/public/html/ |

## LEAD CONTACT AND MATERIALS AVAILABILITY

Further information and requests for reagents may be directed to and will be fulfilled by the Lead Contact, Naihe Jing (njing@sibcb.ac.cn). All materials and reagents will be made available upon installment of a material transfer agreement (MTA).

## EXPERIMENTAL MODEL AND SUBJECT DETAILS

### Mouse strains

Mice were housed in standard cages (No more than five mice in one cage) with a 12 h/12 h light-dark cycle. Every cage was provisioned with the same bedding material (hardwood shavings), and mice were given *ad libitum* access to food and water. The generation of corresponding Nr2f1 point mutant mice was performed as described previously (Wu et al., 2013). Briefly, 3-5 weeks old C57BL/6 female mice were superovulated, and ICR females were used as foster mothers. One-cell-stage embryos were collected and injected with Cas9 mRNAs (50 ng/μl), sgRNA (20 ng/μl), and donor oligo (20 ng/μl). The Cas9 mRNA and sgRNA production was performed as described previously (Wu et al., 2013). Briefly, the pX330 plasmid (Addgene, Plasmid #42230) with T7 promoter was linearized, purified, and transcribed with mMESSAGE mMACHINE T7 ULTRA kit. sgRNAs with T7 promoter were amplified by PCR and transcribed using the MEGAshortscript T7 kit. Finally, the Cas9 mRNA and the sgRNA were purified with the MEGAclear kit according to the manufacturer's instructions. The injected embryos were cultured in KSOM culture medium (Millipore) until the blastocyst stage and transferred into pseudopregnant female mice. The sequences of injected oligonucleotides were listed in Table S4. The C57BL/6 age-matched male mice (over 2-months-age) were used in each behavioral test to avoid hormonal variations (otherwise specified), and were obtained by IVF methods (otherwise specified). Specifically, we obtained sperms from one heterozygous mutant male mouse (C57BL/6 background), and eggs from 8-10 wild-type superovulated female mice (C57BL/6 background). After the *in vitro* fertilization (IVF), the zygotes were transplanted into pseudo-pregnant mice (C57BL/6 background). In all behavior experiments, C57BL/6 background mice were randomized into different groups, and experimenters were blinded to animal genotypes during behavioral tests and data analysis. To prevent odor traces during these tests, every apparatus was carefully cleaned with 75% ethanol and wiped out with paper towels after each test within each experiment. Videos were recorded and analyzed by Noldus Ethovison software. For antagonizing inhibitory transmission, mice were orally administrated with 2 mg/kg Ginkgolide A or vehicle (0.5% methylcellulose +0.2% tween 80), as indicated. All animal studies were performed following the guidelines and regulations of the Institutional Animal Care and Use Committee (IACUC) at the Shanghai Institute of Biochemistry and Cell Biology, CAS, China.

### Cell culture

Human ESC lines (H9 hESCs) (passage 30–45) were maintained in the hESC growth medium (hESCM) and passaged every five days on a feeder layer of irradiated embryonic mouse fibroblasts (derived from CF-1 mouse) as described previously (Thomson et al., 1998). hESC growth medium consisted of DMEM/F12, 20% KSR, 1% GlutaMAX, 1% NEAA, 0.1% β-ME and basic FGF (4 ng/ml). HEK293T cells were maintained in DMEM supplemented with 10% FBS. Human ESC lines (H9 hESCs) and HEK293T cells were obtained from Cell Bank at SIBCB, CAS, China. The generation of mutant (Mut) or reverse mutant (Rev) hESCs were followed by the protocol published before (Ran et al., 2013). Briefly, sgRNA sequence was designed according to the instruction from "http://zlab.bio/guide-design-resources" and cloned to the linearized px330mCherry plasmid (Addgene, Plasmid #98750). PX330-mCherry-sgRNA and corresponding donor templates were transfected into hESCs by Lipofectamine Stem Transfection Reagent followed by the manufacturer's instructions. After 48 hours, mCherry positive cells were collected by BD FACS Aria II and plated in dishes for culture. About ten days later, single clones were picked up manually and sequenced. Primers or oligos were listed in Table S4.

## METHOD DETAILS

### Neuron differentiation

The protocol for hESC neuron differentiation was described previously (Eiraku et al., 2008; Li et al., 2017a; Zhang et al., 2001). Briefly, hESC colonies were digested by collagenase IV (2 mg/ml) and floated in the hESCM without basic FGF. Embryonic bodies (EBs) were formed after four days' suspension and subsequently floated for two days in the neural induction medium (NI medium) consisting of DMEM/F12, 1% N2 supplement, GlutaMAX, NEAA, and β-ME. The EBs then were adhered to a dish coated by Matrigel and cultured in the neuron differentiation medium (ND medium) consisting of 50% DMEM/F12 medium, 50% Neurobasal medium, 1% N2 supplement, 2% B27 without vitamin A, GlutaMAX, NEAA and β-ME for additional 10 days. Then the attached EBs were dissociated into small patches by collagenase IV (0.5 mg/ml) and cultured in ND medium as suspended neural spheres for four days. Finally, these neural spheres were digested with Accutase into single cells and plated on Matrigel-coated dishes in the ND medium supplemented with BDNF (10 ng/ml), GDNF (10 ng/ml) and NT-3 (10 ng/ml) for neuron maturation. For antagonization of the Hedgehog pathway, cells were treated with 2 μM cyclopamine or DMSO, as indicated, during D10–D20 of neuron differentiation.

### RNA extraction and quantitative PCR (qPCR)

Total RNA was extracted from cultured cells or tissues by using the TRIzol reagent, and cDNA was reverse-transcribed, starting from 1000 ng of total RNA with the SuperScript III First-strand cDNA synthesis kit (Invitrogen). qPCR was performed using Mastercycler® RealPlex$^2$ (Eppendorf) and Stormstar SYBR Green qPCR MasterMix (DBI Bioscience). Data were normalized for GAPDH expression. The primers sequences used for qPCR amplification were listed in Table S4.

### Immunofluorescence

Immunofluorescence was performed as described previously (Li et al., 2017a). Samples were fixed with 4% paraformaldehyde in PBS (pH 7.3) for two hours at room temperature and then permeabilized, blocked with 0.25% Triton X-100 /10% donkey serum in PBS for one hour at room temperature. Primary antibodies were diluted in 0.25% Triton X-100 /10% donkey serum in PBS and incubated overnight at 4°C. Samples were washed 0.25% Triton X-100 in PBS three times for 10 min and incubated with secondary antibodies (1:200-1:1000) in 0.25% Triton X-100 /10% donkey serum in PBS for two hours. Primary antibody information was listed in STAR Methods (DLX1/2 primary antibody is a kind gift from Morozov et al. [2009]). Images were taken with Leica TCS SP8 confocal laser-scanning microscope.

### Western blotting

The harvested cells were first washed with cold PBS (without $Ca^{2+}$/$Mg^{2+}$), lysed with 1 × loading buffer, and heated for 10 mins at 100°C. Lysates were centrifuged at 12000rpm at 4°C for 10 min. SDS gel electrophoresis was performed using 20 μg total protein per line, and gels were transferred to nitrocellulose membranes (GE). Nitrocellulose membranes were processed using SuperSignal West Pico Substrate. PageRuler Prestained Protein Ladder was used as the marker.

### Electrophysiology on hESCs-derived neurons *in vitro*

Whole-cell voltage- or current-clamp recording was performed with borosilicate glass micropipettes, which were filled with internal solutions containing the following constituents (in mM): 130 K-gluconate, 20 KCl, 0.2 EGTA, 4 $Mg_2ATP$, 0.3 $Na_2GTP$, 10 HEPES, and 10 $Na_2$-phosphocreatine, at pH 7.3 (290–310 mOsm). Pipette resistance was 3-6 MΩ, and series resistance was typically 20-50 MΩ. Cells were recorded in the artificial cerebral spinal fluid (aCSF) containing the following components (in mM): 125 NaCl, 2 $CaCl_2$, 3 KCl, 2 $MgSO_4$, 1.25 $NaH_2PO_4$, 1.3 $Na^+$-ascorbate, 0.6 $Na_2^+$-pyruvate, 26 $NaHCO_3$, and 11 glucose, at pH 7.4. Step depolarizing currents were injected into cells to record action potentials in the current-clamp mode. For miniature excitatory postsynaptic currents (mEPSCs) recording, the membrane potential was held at −70 mV and mEPSCs were recorded in the presence of tetrodotoxin (TTX, 1 μM) and bicuculline (10 μM). Miniature inhibitory postsynaptic currents (mIPSCs) were recorded in the presence of tetrodotoxin (TTX, 1 μM), CNQX (10 μM) and D-APV (50 μM). For mIPSCs recording, the recording pipette was filled with a Cs-based internal solution containing the following (in mM): 130 $CsMeSO_3$, 1 $MgCl_2$, 1 $CaCl_2$, 10 HEPES, 11 EGTA, 2 $Mg_2ATP$, 0.3 $Na_2GTP$, and 2 QX-314,

at pH 7.3 (290–310 mOsm). And the membrane potential was held at 0 mV. Electrical signals were amplified and filtered at 2–10 kHz (low pass) with Axon MultiClamp 700A (Molecular Devices), digitized at 20–100 kHz (Digidata 1322A; Molecular Devices), and acquired by the pClamp 10 (Molecular Devices). The data were analyzed by the Clampfit 10 and GraphPad Prism 6. Miniature synaptic events were analyzed using MiniAnalysis software (Synaptoosoft, Decator, GA). All experiments were conducted at room temperature.

### Electrophysiology on mouse brain slices *in vivo*

The primary somatosensory (S1) cortical slices from 1 to 2 months (P29-P50) age-matched male mice were prepared as described previously, with some modifications (Lu et al., 2007). In accord with behavioral tests, we only used age-matched male mice to perform electrophysiological experiments. Mice were anesthetized with sodium pentobarbital (50 mg/kg, ip.; Nembutal, Abbott) and transcardially perfused with ice-cold oxygenated aCSF containing the following (in mM): 92 NaCl, 2.5 KCl, 2 $CaCl_2$, 2 $MgSO_4$, 1.2 $NaH_2PO_4$, 5 Na-ascorbate, 3 Na-pyruvate, 2 Thiourea, 20 HEPES, 12 N-acetyl-cysteine, 30 $NaHCO_3$, and 25 glucose, at pH 7.4. After decapitation, brain tissues were dissected and placed in ice-cold oxygenated aCSF. A coronal section was obtained with a vibratome (VT-1200S; Leica), and slices (300 μm thick) were maintained in the incubation chambers with oxygenated (95% $O_2$ / 5% $CO_2$) aCSF at 34°C for thirty mins, and then transferred to room temperature (20-25°C) for at least thirty mins before being transferred to the recording chamber. Whole-cell voltage- and current-clamp recordings were made from layer IV pyramidal cells (PCs) in S1 with an Axon MultiClamp 700A amplifier (Molecular Devices), under an Olympus microscope (BX51WI) equipped with an infrared video camera and differential interference contrast optics. For patch-clamp recording, the single slice was transferred to the chamber perfused with standard aCSF bubbled with 95% $O_2$ / 5% $CO_2$. The recording pipette was filled with an internal solution used the same as *in vitro* electrophysiological recording. To record standard membrane properties and elicit action potentials, a series of step currents (25 pA step increase, up to 1.1 nA, 500 ms duration) were injected into the recorded cell in the current-clamp configuration. For postsynaptic currents recording, the same methods were used except for some changes in the mIPSCs recording process. The internal solution was replaced with a high $Cl^-$ internal solution containing the following (in mM): 10 NaCl, 126 KCl, 1 $MgCl_2$, 10 HEPES, 11 EGTA, 2 $Mg_2ATP$, 0.25 $Na_2GTP$, and 3 QX-314, at pH 7.3 (290–310 mOsm), and mIPSCs were recorded at a holding potential of −70 mV. Electrical signals were amplified and filtered at 2–10 kHz (low pass) with Axon MultiClamp 700A (Molecular Devices), digitized at 20–100 kHz (Digidata 1322A; Molecular Devices), and acquired by the pClamp 10 (Molecular Devices). The data were analyzed with the Clampfit 10 and GraphPad Prism 6. Miniature synaptic events were analyzed by using MiniAnalysis software (Synaptoosoft, Decator, GA). All experiments were conducted at room temperature.

### Library preparation, data processing, and data analysis for RNA-Seq

Total RNA was extracted and subjected to quality control and quantification. For each sample, poly-A containing mRNA was purified using poly-T magnetic beads and subsequently submitted to the first strand and second-strand synthesis (E7525L and E6111L, NEB). cDNA libraries were generated using the NEBNext Ultra DNA Library Prep Kit for Illumina (E7370S, NEB). High-throughput sequencing was performed on a HiSeq instrument at the Berry Genomics Co, Ltd. Gene expression levels were calculated by HISAT2 (version 2.1.0) and FeatureCounts (version 1.5.3) (Sahraeian et al., 2017) with the reference hg19. The differentially expressed genes (DEGs) were identified by DESeq2 (version 1.16.1) (Love et al., 2014) (padj < 0.05, foldchange > 2). For BrainSpan correlation analysis, correlation between our RNA-Seq samples and the BRAINSPAN database (n = 524 brain samples across all ages) was used to classify the samples as corresponding to a particular brain region and developmental age. The common genes were matched within our set with the ones for which expression levels were available within the BrainSpan dataset. The Pearson correlation matrix between the log-transformed (log2 (FPKM + 1)) expression levels of our samples and each of the BrainSpan samples was computed, and the top 5 correlated samples were listed. For functional enrichment analysis, DEGs' functional enrichment analysis, including GO (Gene Ontology) and KEGG (Kyoto Encyclopedia of Genes and Genomes) pathway enrichment, were performed using clusterProfiler (version 3.4.4) (Yu et al., 2012). For target gene enrichment analysis for different signaling pathways, in addition to the signaling pathways (TGF-β, Hedgehog, BMP, FGF, Nodal, and WNT) analyzed previously (Li et al., 2017a; Peng et al., 2016), two other signaling pathways (Notch and Hippo/Yap) were included in this analysis. Rank Prod ($p < 0.001$ for Notch and $p < 0.01$ for Hippo/Yap) results were generated using data from public datasets GSE15268 and GSE69669, respectively. For gene set enrichment analysis (GSEA), the published GEO dataset (GSE) for the Hedgehog signaling pathway perturbations was assessed by comparing control samples with treatment samples using RankProd (version 3.2.0, p value $\leq 0.001$) (Hong et al., 2006) to identify the potential signaling target genes of Hedgehog pathway. Conserved genes in humans were selected as the target genes of the Hedgehog signaling pathway (Li et al., 2017a; Peng et al., 2016). To determine the enrichment of the pathway target genes in WT or Mut cells, GSEA (Mootha et al., 2003; Subramanian et al., 2005) was used to evaluate whether a specific signaling pathway target gene set is significantly enriched in WT or Mut cells. The target gene sets of the Hedgehog signaling pathway were used as the test gene sets to run GSEA (FDR < 25%).

### Library preparation, data processing, and data analysis for ChIP-Seq

The protocol for chromatin immunoprecipitation (ChIP) was described previously (Yang et al., 2018). Briefly, cross-linked cells were lysed in lysis buffer, and the samples were sheared for 14 cycles (30 s on/off) in a Bioruptor Pico (Diagenode, Belgium) to achieve an average fragment size of 200-300 bp. Solubilized fragmented chromatin was immunoprecipitated with Anti-FLAG® M2 Magnetic Beads (M8823, Sigma-Aldrich). Antibody-chromatin complexes were pulled down using a magnetic separation rack, washed several

times, and then eluted from the magnetic beads. Reverse crosslink was performed subsequently under 65°C for at least 4 hours. ChIP-DNA was treated with RNase A and Proteinase K, precipitated with ethanol. ChIP-DNA was finally solved in nuclease-free water and quantified using Qubit (Thermo). Sequencing libraries were generated by using the NEBNext Ultra DNA library preparation kit (E7370, NEB). Libraries were quality-controlled and quantified using a Qubit 2.0 Fluorometer (Life Technologies) and Agilent 2100 Bioanalyzer (Agilent Technologies). High-throughput sequencing was performed on the Illumina HiSeq instrument at the Berry Genomics Co, Ltd. Clean reads were mapped with Bowtie2 (version 2.3.1) (Langmead and Salzberg, 2012), then the peaks were called using MACS2 (version 2.1.1) main program ($q < 0.05$) (Zhang et al., 2008). MACS2 bdgcmp was used to generate the log LR track, then the bedGraph files for the log LR track were converted to bigWig files. Correlations between biological replicates were calculated with wigCorrelate, and then the biological replicates were merged with MACS2. All the above were run with default parameters. Further analysis was performed with GREAT software (McLean et al., 2010).

### Luciferase assay

H9 hESCs-derived NPCs cultured in 24-well plates were transfected with 500 ng pGL3-luciferase reporters, 100ng pcDNA3.1$^{+}$-WT/Mut NR2F1, 50 ng pRL-TK per well. 48 hr after transfection, the luciferase activity was measured by Dual-Glo$^{TM}$ luciferase assay system in triplicates.

### Tissue processing, immunohistology, and imaging

This section was conducted by the protocol published previously (Feng et al., 2017). Briefly, mice were anesthetized with chloral hydrate (400 mg/kg) and perfused with 50 mL of sodium phosphate-buffer and then with 50 mL of 4% paraformaldehyde in 1X PBS. And then the brains were carefully isolated, fixed with 4% paraformaldehyde overnight at 4°C. Brain tissues were dehydrated through a series of graded ethanol baths, xylene solutions, and then infiltrated with paraffin. Finally, brains were embedded in paraffin, coronal brain sections (7 um thickness) were generated using a Leica RM2235.

For immunohistology staining, the slides were dewaxed and rehydrated. Then the slides were washed in double-distilled water and PBS with 1 min each. The slides were treated with boiling antigen retrieval solution for 15 min. And then the slides were rinsed with PBS for 10 min three times. The slides were treated with 3% $H_2O_2$ in PBS for 30 min and then washed with PBS for 10 min three times. Next, the sections were incubated with blocking buffer containing 1% BSA, 5% serum in PBS for one hour, and then incubated with the primary antibody in hybridization buffer overnight at 4°C. After being washed with PBS for 10 min for three times, sections were incubated with secondary antibody for one hour at room temperature. The sections were washed and counterstained with DAPI. After washing, the slides were mounted with mounting medium. In some experiments, TSA kit (Invitrogen) was used. The samples were treated as same as the regular immunofluorescence staining until the completion of the primary antibody incubation. Then, the processes were carried out with TSA kit by following the manufactory's protocol. The primary antibodies used in the study were listed in STAR Methods. The following secondary antibodies were used in the study: Donkey anti-rabbit IgG biotin-conjugated (1:400); Donkey anti-Rat IgG (H+L) biotin-conjugated (1:400). A series of z stack microscopy fluorescent images were captured by using a digital fluorescence microscope (Olympus BX51) or confocal laser-scanning microscope (Leica TCS SP8).

### Mouse behavioral tests

#### *Three-chamber test*

Briefly, the arena consisted of a transparent box which was divided into three chambers of the same size and removable doors in each chamber. Each mouse, including the test mouse and age/gender-matched C57BL/6 wild-type mice, not littermates, were kept in the test room individually one hour before the experiment. Two wire cups were placed in the corner of the left and right chambers. The test mouse was introduced to the central chamber and was allowed to get access to three chambers for 10 min. In the first stage, a strange mouse, which was age/gender-matched C57BL/6 wild-type mice, not littermates, was introduced into the wire cup of the left or right chamber, an inanimate object was placed into the other wire cup. The test mouse was allowed to get access to three chambers and both wire cups within 10 min. The time of test mouse spent in interacting with the stranger mouse or an inanimate object was recorded. The chamber was cleaned with 75% ethanol after each test. In the second stage, the inanimate object was replaced with another novel age/gender-matched C57BL/6 wild-type mice, but not littermates. The test mouse was allowed to get access to three chambers and both wire cups within 10 min. The time of test mouse spent in interacting with the familiar mouse or a stranger mouse was recorded. The preference index was calculated as below: Preference index = (time spent in interacting with the novel mouse)/ (time spent in interacting with the novel mouse + time spent in interacting with object/familiar mouse)*100%.

#### *Self-grooming test*

The mice were first habituated in a clean chamber individually for 10 min. The time spent in self-grooming was recorded within 10 min. Self-grooming included actions of face-wiping, scratching of head, neck or ears and full-body grooming.

#### *Y-maze test*

The Y-maze apparatus consisted of three identical arms (40 × 5 cm with 10 cm high walls). Spontaneous alternation behaviors were assessed. The test mouse was allowed to explore the Y-maze for 8 min freely, and arms choices (all four paws entering one arm) were recorded by a camera. Overlapping triplets of 3 arm visits were counted as one complete spontaneous alternation. The score was calculated as the following formula: (number of spontaneous alternation)/ (total number of arm visits – 2) *100%.

### *Open-field test*

The test mouse was first allowed to explore in the open-field apparatus for 5 min. After washing the apparatus with 75% ethanol, the test mouse was introduced into the apparatus again and allowed to explore for 8 min. The time spent in the center region of the apparatus and distance traveled in the apparatus were calculated.

### *Elevated plus maze*

The test mouse was introduced into the intersection of closed and open arms of the elevated plus maze apparatus and allowed to explore for 5 min. The time spent in closed or open arms were collected.

### *Dark-light emergence test*

The apparatus was divided into two connected sections-dark chamber and light chamber. The test mouse was placed into the apparatus and allowed to explore for 10 min. The total time spent in the light and dark chamber were measured.

### *Rotarod test*

Rotarod apparatus was used to examine the motor coordination of a mouse. The test mouse had been tested three trials once a day for three days with the rod rotation increasing from 4 to 40 rpm in 5 min. The interval of each trial was 30 min. The rotarod apparatus was stopped once the test mouse fell, and the latency to fall off the rod was determined, the average latency of three trials once a day was calculated.

### *2-object novel object recognition test*

The test was modified from previous protocols (Huang and Hsueh, 2014; Leger et al., 2013). Briefly, the whole test was a 3-days-trial, consisting of habituation, training, and test stage. In the training stage, two identical objects were placed in the apparatus. Mice were allowed to explore in the apparatus for 10 mins. In the test stage, one of those objects was replaced with another, but not identical, novel object (N). Mice were allowed to explore in the apparatus for 10 mins. The time in exploration of different objects (familiar object (F) or novel object (N)) in the test stage was calculated. The preference for novel object was calculated as followings: Preference index = exploration time of novel object/(time in exploration of novel object + time in exploration of familiar object)*100.

## QUANTIFICATION AND STATISTICAL ANALYSIS

### Counting analysis on brain slices

For analysis of mouse primary somatosensory cortex or prefrontal cortex *in vivo*, several sections of the primary somatosensory or prefrontal cortex along the rostro-caudal axis were used, and the numbers of $Cux1^+$, $Ctip2^+$, $GluR2^+$ cells were counted in per $mm^2$. $Gad1^+$, $PV^+$, $SST^+$, and Gad1-$GFP^+$ cells were counted in each field or per $mm^2$. All quantifications were performed with more than ten brain sections from at least three pairs of mice.

### qPCR analysis

PCR data of gene expression were normalized to internal reference Gapdh and the relative mRNA level was quantified with the $2^{-\Delta\Delta Ct}$ methods. Data from at least three independent induction batches were used for statistical analysis.

### Statistical analysis

For qPCR, ChIP-qPCR, and luciferase assay, an average value was calculated from at least three independent replicates. For statistical analysis of positive immunostaining cells, an average percentage was calculated from at least ten independent fields. All data were obtained from at least three independent experiments. GraphPad Prism software was used to determine statistically significant differences. Data were presented as mean ± SEM. Student's t tests were used to compare the effects of different two groups. One way-ANOVA tests were used to compare the effects of different three or more groups. Differences were considered statistically significant at * $p < 0.05$, * * $p < 0.01$, * * * $p < 0.001$.

## DATA AND CODE AVAILABILITY

The accession number for RNA- and ChIP-Seq data in this paper is GEO: GSE132965. The link is https://www.ncbi.nlm.nih.gov/geo/query/acc.cgi?acc=GSE132965.